



# Neoproterozoic tectonic transition from subduction-related convergence to continental extension of the Tarim Block, NW China

Zihui Cai<sup>a</sup>, Bizhu He<sup>a,b</sup>, Joseph G. Meert<sup>c</sup>, Xuxuan Ma<sup>a,b,\*</sup>, Cunli Jiao<sup>d</sup>, Ruohan Liu<sup>a</sup>, Xijie Chen<sup>e</sup>, Xiaorui Yun<sup>a</sup>

<sup>a</sup> Key Laboratory of Deep-Earth Dynamics of Ministry of Natural Resources, Institute of Geology, Chinese Academy of Geological Sciences, Beijing 100037, China

<sup>b</sup> Southern Marine Science and Engineering Guangdong Laboratory, Guangzhou 511458, China

<sup>c</sup> Department of Geological Sciences, University of Florida, 241 Williamson Hall, Gainesville, FL 32611, USA

<sup>d</sup> Exploration and Production Research Institute of SINOPEC, Beijing, China

<sup>e</sup> Development and Research Center of China Geological Survey, Beijing 100037, China

## ARTICLE INFO

### Keywords:

Neoproterozoic  
Mafic dike  
Magmatism  
Tectonic transition  
Extension  
Tarim Block

## ABSTRACT

The Tarim Block, one of the three largest cratons in China, plays an important role in the reconstruction of the Rodinia supercontinent. Knowledge of the Neoproterozoic tectonic evolution of the Tarim Block, especially the tectonic transition from convergence to rifting, remains unclear. The Aksu terrane, an integral part of the Tarim Block, is marked by the occurrence of Neoproterozoic blueschists, conglomerates, and mafic rocks that may provide important constraints on its tectonic history. We present an integrated study involving detailed field observations, whole-rock geochemistry, and zircon U-Pb geochronology for rhyolitic clasts in a Neoproterozoic conglomerate, a syenite pluton and mafic rocks in the Aksu region. Zircon U-Pb dating of the rhyolite yielded a crystallization age of  $840 \pm 4$  Ma. Geochemically, the rhyolite is characterized by enrichment of light rare earth elements and depletion of high field strength elements, indicating a subduction-related arc setting. Syenites interspersed with mafic intrusions were crystallized at  $\sim 755$  Ma, representing fractional crystallization products from intra-plate mantle-derived basaltic magma. Based on a compilation of previous studies, we find that the Late Neoproterozoic–Early Cambrian mafic rocks in the Aksu region can be divided into three phases. Phase I mafic intrusions ( $\sim 760$ –745 Ma) occurring as dikes intruded into the blueschist-bearing Aksu Group. Phase II mafic intrusions ( $\sim 755$  Ma) intruded into the Neoproterozoic Qiaoenbulake Formation. Phase III mafic rocks ( $\sim 520$  Ma) are sills or basalts hosted within the Sugaitebulake Formation. Detailed studies suggest that subduction of oceanic lithosphere in the Aksu area persisted until at least  $\sim 840$  Ma. The transition from ocean-continent subduction to continental extension took place around ca. 760 Ma. At 755 Ma, the northwestern Tarim region experienced significant extension.

## 1. Introduction

Rodinian crustal fragments in China consist primarily of the North China, South China, and Tarim Blocks along with myriad microcontinents. The Tarim Block in northwestern China hosts the Tarim Basin with an area of  $>560,000$  km $^2$ . It is fringed by mountain ranges and intermontane basins including the Tianshan belt, Kuluketage, Aksu, Tiekelike, and Altyn blocks along its northern, northeastern, northwestern, southwestern, and southeastern margins, respectively (Fig. 1). The Precambrian crystalline basement of the Tarim Block is overlain by

3–6 km of Phanerozoic-aged unmetamorphosed sedimentary cover (Jia, 1997). The Tarim Block has an early Archean nucleus intruded by late Archean to Paleoproterozoic igneous rocks (Hu and Wei, 2006; Lu et al., 2008; Shu et al., 2011; Long et al., 2010, 2011a; Zhang et al., 2012a, 2012b, 2013a, 2013b; Xu et al., 2013a; Ge et al., 2018, 2020; Cai et al., 2018; Lv et al., 2020). There is a general agreement that the  $\sim 2.1$ – $1.8$  Ga orogenic event in Tarim corresponds to the assembly of the Paleo-Mesoproterozoic Columbia or Nuna supercontinent (e.g., Zhang et al., 2007, 2012b; Shu et al., 2011; Zhu et al., 2011; Lei, et al., 2011; Long et al., 2012; Ma et al., 2012, 2013, 2014; Wu et al., 2012; Zhao and

\* Corresponding author at: Key Laboratory of Deep-Earth Dynamics of Ministry of Natural Resources, Institute of Geology, Chinese Academy of Geological Sciences, Beijing 100037, China.

E-mail address: [xuxuan.ma@hotmail.com](mailto:xuxuan.ma@hotmail.com) (X. Ma).

Cawood, 2012; Xu et al., 2013a; Gao et al., 2015; Ge et al., 2014a, 2014b, 2015; Wang et al., 2014a, 2014b; Cai et al., 2020). The ~1.75 Ga magmatic episode in Tarim reflects an early breakup event of the Columbia supercontinent (Yu et al., 2013; He et al., 2013).

The Neoproterozoic tectonic evolution of the Tarim Block is contentious. One of the controversial topics pertains to the origin and tectonic setting of Early Neoproterozoic granitoids (e.g., Xu et al., 2005, 2013a, 2013b; Zhang et al., 2006, 2007, 2009a, 2011; Lu et al., 2008; Shu et al., 2011; Long et al., 2011b; Wu et al., 2012, 2018; Wang et al., 2015; Yu et al., 2019; Peng et al., 2019). Were these granitoids related to continent–continent collision during the assembly of Rodinia supercontinent (e.g., Zhang et al., 2006, 2011; Xu et al., 2005, 2013a; Lu et al., 2008; Long et al., 2011b; Shu et al., 2011; Wu et al., 2012) or were they related to a circum-supercontinent subduction at the periphery of Rodinia (Ge et al., 2016; Cai et al., 2019)? These issues arise, in part, due to the lack of a precise location for Tarim within Rodinia (Meert, 2014; Wen et al., 2017; Wang et al., 2020; Ren et al., 2020).

The Middle to Late Neoproterozoic igneous rocks (most of which are mafic) are commonly considered to have been formed during rifting in the Tarim Block (Xu et al., 2005, 2013a, 2013b; Zhang et al., 2006, 2007, 2009a, 2009b, 2011, 2012a, 2012c, 2012d; Zhu et al., 2008; Lu et al., 2008; Long et al., 2011a; Shu et al., 2011; Wang et al., 2010, 2014c, 2015; Lei et al., 2013; Ge et al., 2016; Wu et al., 2018). However, knowledge of the Neoproterozoic tectonic transition from convergence to rifting remains unclear. Herein, the second controversy we hope to address in this paper is to establish the timing and mechanism for the transition from an ocean-continent subduction-related convergent regime to an extensional regime.

The Aksu terrane is located in the northwestern portion of the Tarim Block, where Precambrian rocks are well exposed (Figs. 1 and 2). The presence of Neoproterozoic blueschists in the Aksu region, indicates subduction and accretion processes occurred along the northwestern margin of the Tarim Block during the Neoproterozoic (Liou et al., 1989, 1996, 2004; Nakajima et al., 1990; Zhu et al., 2008; Zhang et al., 2009a, 2012c; Yong et al., 2013; Lu et al., 2018). Some Late Neoproterozoic mafic rocks, especially basalts, mafic dikes and sills, formed in an

continental rift setting in the Aksu and Kuluketage areas (e. g., Liou et al., 1989, 1996, 2004; Nakajima et al., 1990; Zhu et al., 2008; Zhang et al., 2009a, 2009b, 2012c; Yong et al., 2013). Herein, we conducted integrated analyses on Neoproterozoic igneous samples including rhyolite, syenite, and mafic rocks in the Aksu region. Our results placed new constraints on the tectonic transition from Neoproterozoic oceanic subduction to continental rifting in the northwestern Tarim Block.

## 2. Geological setting and field descriptions

In Aksu region, the Precambrian rocks comprise the metamorphic Aksu Group and unmetamorphosed Neoproterozoic sequences. The Aksu Group includes blueschist, greenschist and metagreywacke, intruded by mafic dikes. The Neoproterozoic sequences consist of the Qiaoenbulake (or Qiaoenbrak), Yuermeinake (or Yuermeinak), Sugai-tebulake (or Sugetbrak), and Qigebulake (or Qigebra) Formations from oldest to youngest (Figs. 2 and 3).

The Aksu Group is best exposed in the Aksu and Wushi regions (Figs. 1 and 2). The peak metamorphic condition of Aksu blueschist has been estimated to be 350–450 °C and 5.5–7.0 kbar (Liou et al., 1996). The Aksu Group is significantly deformed (Fig. 4) with foliations (Fig. 4a–c, e–g), lineations (Fig. 4d) and folds (Fig. 4a and h). In the western and southern areas of Aksu, a series of NE-SW trending folds range from macroscopic to 10-km-wavelength in scale (Figs. 2 and 4a). NW-SE striking and steeply dipping (65–90°) unmetamorphosed mafic dikes cross-cut the large-scale folds (Fig. 4a) and other deformed rocks in Aksu Group (Figs. 2 and 4b and d). The detrital zircon U-Pb, whole-rock Sm-Nd and Ar-Ar dating results provided various ages for the blueschist protolith, ranging from ~890 to 730 Ma (e.g., Zhang et al., 2009a; Zheng et al., 2010; Yong et al., 2013; Lu et al., 2018; Xia et al., 2019). An <sup>40</sup>Ar/<sup>39</sup>Ar age of 750 Ma from the Aksu schists, constrains the metamorphic age of the Aksu blueschist to ~750 Ma (Yong et al., 2013). Zircon U-Pb and Ar-Ar studies constrain the timing of dike emplacement to ~760 Ma (Zhang et al., 2009a; Xia et al., 2019) and to 745 Ma (Lu et al., 2018), respectively.

The Qiaoenbulake Formation (1600–2040 m in thickness) consists of

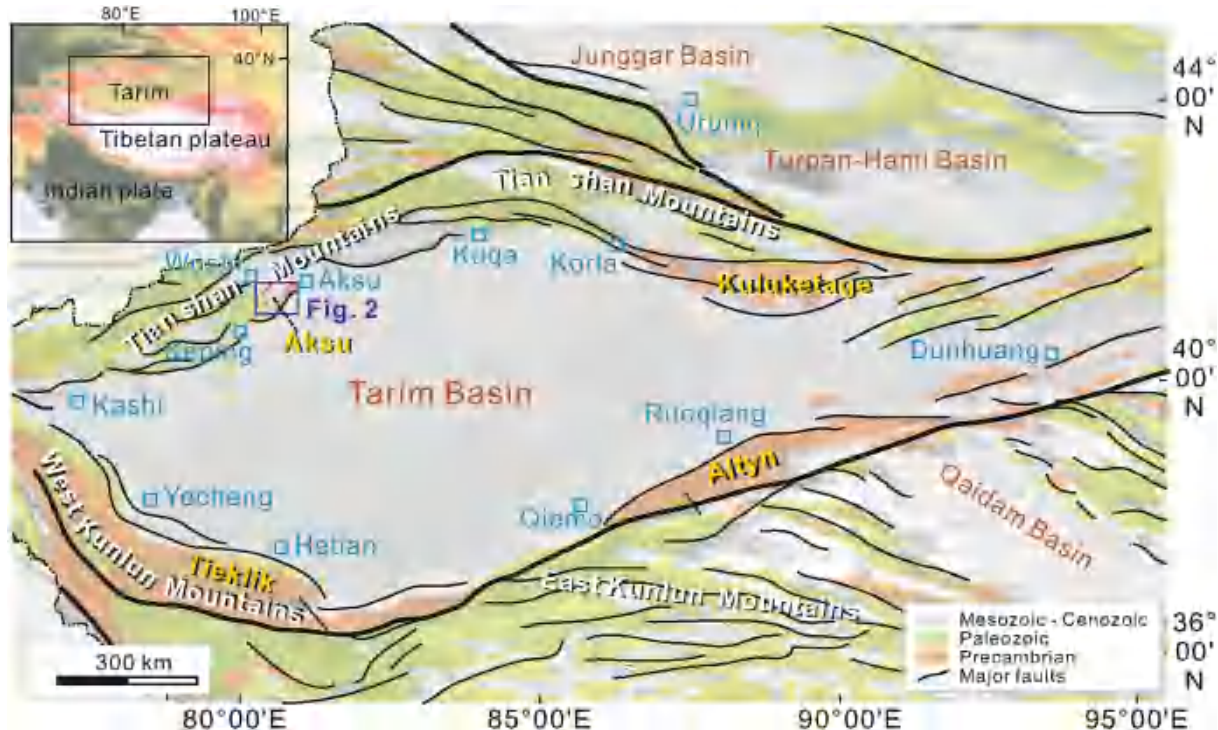


**Fig. 1.** Simplified geological map of the Tarim Block and adjacent area (modified from Xu et al., 2013a) showing sampling locations. The inset map shows the location of the Tarim Block, adjacent to the Tibetan Plateau.

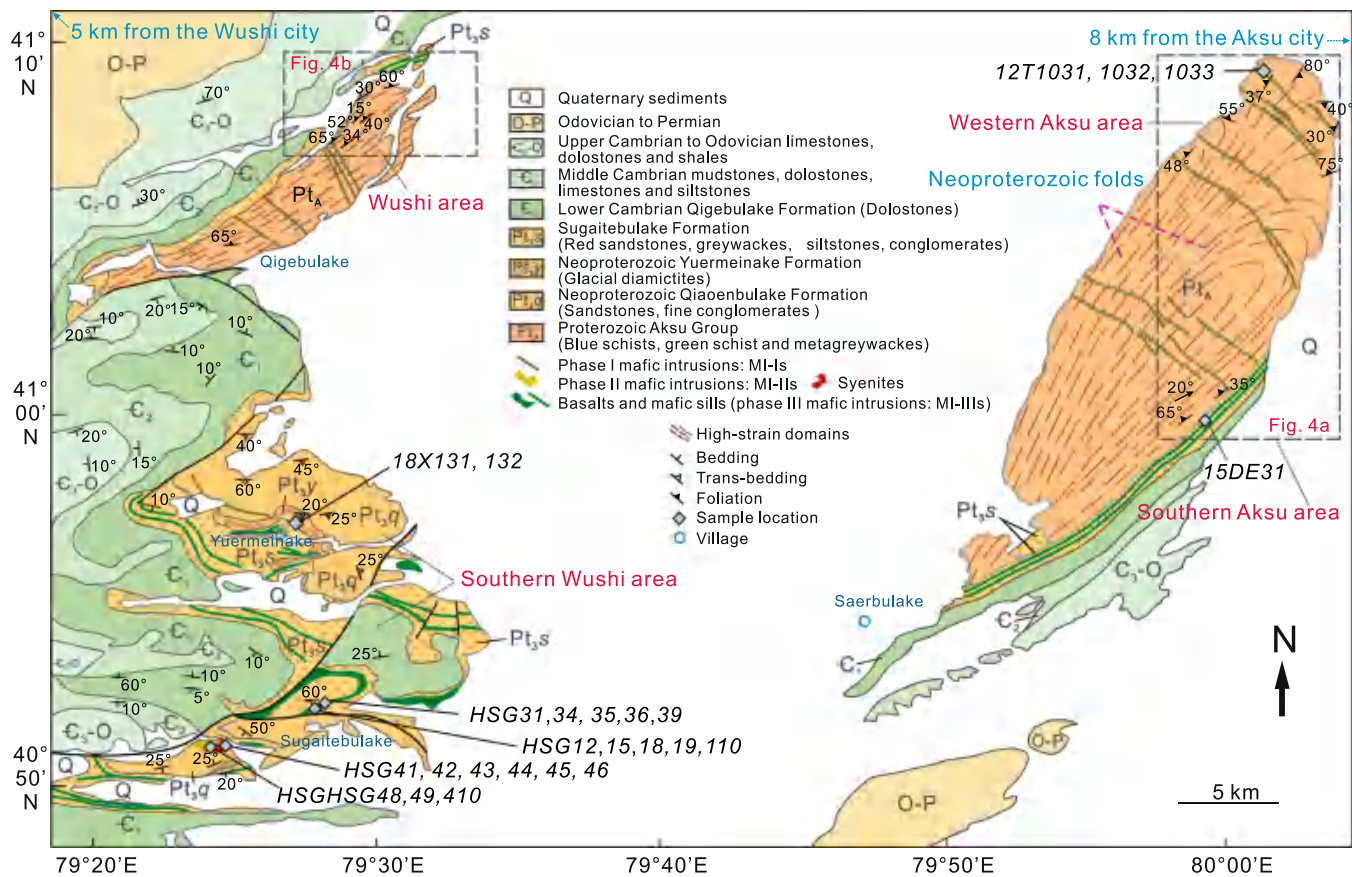


**Fig. 2.** Simplified geological map of the Aksu region (modified after XBGMR, 1966) showing the sampling locations.

~2 km of marine sandstone and conglomerate (Gao and Chen, 2003; Gao et al., 2013; Yang et al., 2014; Wu et al., 2018; He et al., 2021) (Figs. 2 and 3) and has a maximum depositional age of ~781 Ma (He et al., 2014). In some locations, the Qiaoenbulake Formation is slightly metamorphosed. It was previously regarded as the lowest unit within the unmetamorphosed Neoproterozoic sequence. A ~900 Ma andesite with arc affinities has been reported beneath the Qiaoenbulake Formation (He et al., 2019a). In the southern Wushi area, a large mafic intrusion emplaced into the Qiaoenbulake Formation (Figs. 2, 5a–c). Syenite plutons and veins occur near the mafic rocks (Figs. 2, 5a–c). No sharp contact or obvious chilled margin exists between the mafic and syenite plutons (Figs. 2, 5a–c), suggesting that they are coeval and represent a suite of bimodal igneous rocks in the Aksu region.

The Yuermeinake Formation unconformably overlies the Qiaoenbulake Formation and is composed of <70 m-thick glacial diamictites, including poorly sorted sandstone and conglomerate (Figs. 2, 3, 5d; Gao and Chen, 2003; Wen et al., 2015; Wu et al., 2018). Clasts within the conglomerate, including schist, sandstone (Fig. 5e), and volcanic rocks (Fig. 5f). The clasts are typically large (up to 1.5 m) and angular (Fig. 5e–f), suggesting derivation from a nearby source.

The Yuermeinake Formation in the Wushi area and the southern Aksu region, is unconformably overlain by the Sugaitebulake Formation (Figs. 2, 3, 4a–b, e–f, 5d). The Sugaitebulake Formation is ~400–450 m in thickness and consists of a basal conglomerate (alluvial fan), fluvial and lacustrine facies sandstone and siltstone formed in a non-marine sedimentary environment (Turner, 2010). Some basalt layers occur in the Sugaitebulake Formation in the southern Aksu and southern Wushi areas (Figs. 2 and 5g–j). Mafic sills locally intrude the Sugaitebulake Formation (Figs. 2, 3, 5k–m). In contrast, mafic dikes in the Aksu Group do not intrude the Sugaitebulake Formation (Fig. 4a–b). The crystallization ages of the basalts/mafic sills in the Sugaitebulake Formation were reported to be ~783 Ma (Zhang et al., 2012c) or ~615 Ma (Xu

et al., 2013b) based on zircon U-Pb analyses. Considering the morphology characteristics, the zircons were probably xenocrysts, and the crystallization age of the mafic rocks might be younger than (783 Ma or 615 Ma) (e. g., Lu et al., 2018). Ar-Ar dating results constrain the crystallization timing of the basalts/sills in the Sugaitebulake Formation (MI-IIIs) to ~520 Ma (Lu et al., 2018).

For convenience, we refer to the mafic dikes in the Aksu Group (Figs. 2, 3, 4a–b, d), the mafic pluton in the Qiaoenbulake Formation (Figs. 2, 3, 5a–c), and the basalts/mafic sills in the Sugaitebulake Formation (Figs. 2, 3, 5g–m) as phase I mafic intrusions (MI-Is), phase II mafic intrusions (MI-IIs) and phase III mafic intrusions (MI-IIIs), respectively.

### 3. Petrography

In this study, we collected rhyolite clasts from a conglomerate within the Yuermeinake Formation (Fig. 5f). The volcanic clasts are large (>10 cm in length) and porphyritic in texture. The rhyolite is composed of plagioclase (50–60%), quartz (30–35%) and hornblende (5%) (Fig. 6a–b).

MI-Is dikes are composed of feldspar (50–60%), clinopyroxene (30–35%) and hornblende (5–10%), with a few accessory minerals such as magnetite and zircon (Fig. 6c). The MI-IIIs are medium- to coarse-grained with gabbroic texture (Fig. 6d). Mineral assemblages are plagioclase (45–55%), clinopyroxene (30–35%) and Fe-Ti-oxide (5%), with rare zircon and apatite (Fig. 6d). The MI-IIIs are porphyritic or diabasic porphyritic texture (Fig. 6e–h), and consist of plagioclase (55–60%) and clinopyroxene (25–30%), with subordinate amphibole, biotite, orthopyroxene, and minor accessory Fe oxides (Fig. 6e–h). The syenite samples are medium- to coarse-grained, equigranular and consist of orthoclase (70–75%), clinopyroxene (10–15%), and quartz (5%) (Fig. 6i–j).

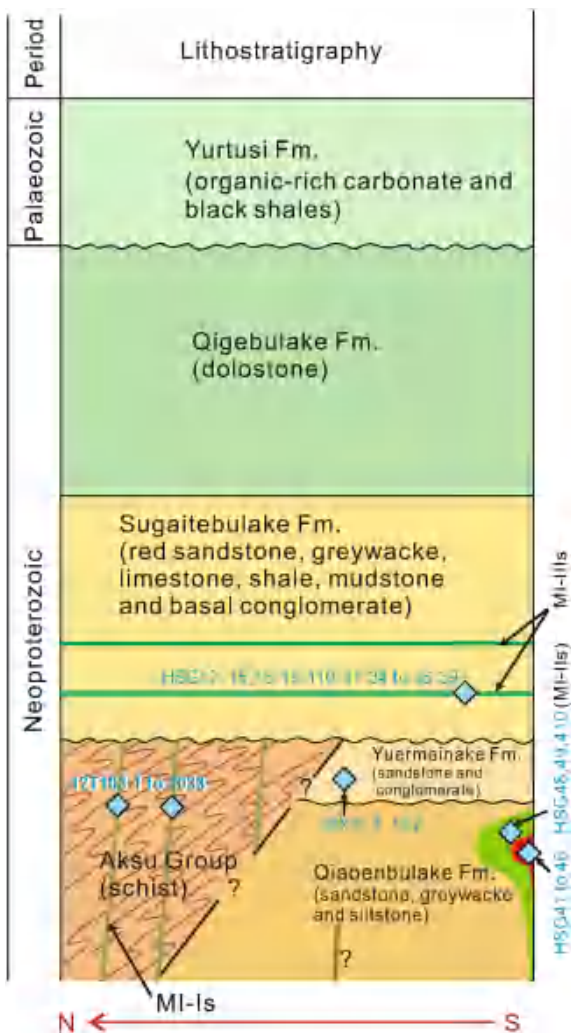


Fig. 3. Simplified stratigraphic column of the Neoproterozoic to Early Cambrian in the Aksu region (modified after Turner, 2010).

#### 4. Analytical methods

Zircon U-Pb dating was conducted by laser-ablation inductively-coupled-plasma mass spectrometry (LA-ICP-MS) after cathodoluminescence (CL) imaging. The LA-ICP-MS analyses were carried out at the Institute of Mineral Resources, Chinese Academy of Geological Sciences (CAGS), Beijing, China. We use FEI PHILIPS XL30 SFESEM and Thermo Finnigan Neptune MC-ICP-MS and Analytik Jena PQMS Elite ICP-MS instruments. Detailed operating conditions for the laser ablation system and the ICP-MS instrument and data reduction follow the methodology in Hou et al. (2007) and Hou et al. (2009). The off-line selection and integration of background and signals, and time-drift correction and quantitative calibration for U-Pb dating were performed using ICPMSDataCal (Liu et al., 2010). Zircon GJ-1 was used as the external standard, with preferred U-Th-Pb isotopic ratios from Jackson et al. (2004). The uncertainty of the preferred values (0.5%) for the external standard GJ-1 was propagated into the possibilities for the analyzed samples. U, Th, and Pb concentrations of zircon were calibrated using NIST 610. Concordia diagrams and age calculations were conducted using Isoplot/Ex\_ver3 (Ludwig, 2003). The detailed geochronological results are listed in Table S1.

Whole-rock major and trace element concentrations were obtained using X-ray fluorescence (XRF) and ICP-MS, conducted at the National Research Center for Geoanalysis, CAGS. Major elements analyzed by XRF have analytical uncertainties of <5%. Trace elements were

separated using cation-exchange techniques and have analytical uncertainties of 10% (element concentrations <10 ppm) and ~5% (element concentrations >10 ppm) (Zeng et al., 2012).

Sr-Nd isotopic compositions were determined at the Beijing Createch Testing Technology Co., Ltd. Samples were dissolved in  $\text{HNO}_3$  and HCl for Sr or Nd purification. Sr was separated and purified using Sr-Spec (Triskem, 100–150  $\mu\text{m}$ ) resin. Sr-Nd was separated by conventional cation-exchange technique. Isotopic compositions of Sr and Nd were measured using a Thermo Fisher Scientific Neptune Plus MC-ICP-MS. Sr and Nd ratios were corrected for instrumental mass fractionation based on  $^{88}\text{Sr}/^{86}\text{Sr} = 8.375209$  and  $^{146}\text{Nd}/^{144}\text{Nd} = 0.7219$ , respectively. The detailed analytical methods are described in Yang et al. (2010). For accuracy monitoring, the Sr isotope standard NBS 987 and Nd isotope standard GSB-Nd were tested and yielded an average  $^{87}\text{Sr}/^{86}\text{Sr} = 0.710248 \pm 10$  (2SD,  $n = 17$ ) and an average  $^{143}\text{Nd}/^{144}\text{Nd} = 0.512179 \pm 18$  (2SD,  $n = 21$ ).

#### 5. Analytical results

##### 5.1. Zircon U-Pb dating

One rhyolitic clast sample (18X131) in the Yuermeinake Formation and two syenite samples (HSG46 and HSG47) (Fig. 2) were dated through zircon LA-ICPMS U-Pb dating (Table S1). Representative zircon CL images and corresponding analytical spots are shown in Fig. 7.

Zircon grains in the rhyolitic clast sample (18X131) are euhedral and prismatic in shape, 50–200  $\mu\text{m}$  in length, and exhibit oscillatory zoning as well as high Th/U ratios (0.3–1.8). A total of 20 analyses yielded a weighted mean  $^{206}\text{Pb}/^{238}\text{U}$  age of  $840 \pm 4$  Ma ( $n = 20$ , MSWD (mean squared weighted differences) = 0.1) (Fig. 7a and b). This age is interpreted as the crystallization age of the rhyolite.

Nineteen and eighteen zircon grains from the samples HSG46 and HSG47 were analyzed, respectively. These zircon grains are prismatic (~60–200  $\mu\text{m}$  long) with aspect ratios of 1:1–2:1, showing clear oscillatory zoning. Th/U ratios range from 0.7 to 2.2. These observations are indicative of magmatic origin (Hoskin and Schaltegger, 2003). A total of 19 zircon grains from HSG46 yielded a weighted mean  $^{206}\text{Pb}/^{238}\text{U}$  age of  $754 \pm 4$  Ma (MSWD = 0.3) (Fig. 7c and d) and 18 zircon grains from the HSG47 yielded a weighted mean  $^{206}\text{Pb}/^{238}\text{U}$  age of  $755 \pm 5$  Ma (MSWD = 0.3) (Fig. 7e and f). These are crystallization ages of the syenites.

##### 5.2. Whole-rock geochemistry

Analysis of major and trace elements reveals that the rhyolite clasts from the Youermeinake Formation have  $\text{SiO}_2$  contents of 71 wt% (Figs. 8 and 9) and  $\text{K}_2\text{O} + \text{Na}_2\text{O}$  contents of 6 wt%, and plot in the rhyolite field on the  $(\text{K}_2\text{O} + \text{Na}_2\text{O})/\text{SiO}_2$  diagram (Fig. 8). Based on the molar ratios of  $\text{Al}_2\text{O}_3/(\text{CaO} + \text{Na}_2\text{O} + \text{K}_2\text{O})$  (A/CNK) and  $\text{Al}_2\text{O}_3/(\text{Na}_2\text{O} + \text{K}_2\text{O})$  (A/NK), the rhyolites are metaluminous (Table S2). These two samples have similar chondrite-normalized REE patterns and are characterized by enriched light rare earth elements (LREEs) ( $[\text{La}/\text{Yb}]_N$  values are 6.59 and 6.73, respectively), flat HREEs and slightly negative Eu anomalies ( $\text{Eu}/\text{Eu}^* = 0.8$ ) (Fig. 10a). In the primitive mantle-normalized trace element diagram (Fig. 10b), they show depletion in high field strength elements (HFSEs) such as Nb, Ta and Ti compared to Zr and Hf, indicating the concentration of residual amphibole and Ti-bearing minerals in the magmatic source.

Three samples (12T1031, 12T1032 and 12T1033) of mafic dikes in the Aksu Group (MI-Is) plot in the alkaline series field on the diagram of  $\text{K}_2\text{O} + \text{Na}_2\text{O}$  versus  $\text{SiO}_2$  (Fig. 8). The major oxides Ti, total Fe, Ca and P showed a decreasing trend with increasing  $\text{SiO}_2$  (Fig. 9). The MI-Is have total rare earth element (REE) contents of 237–255 ppm and are enriched in large-ion lithophile elements (LILE) such as Rb, Ba, and Th, depleted in HFSEs with marked negative Nb and Ta anomalies (Fig. 10c and d). Two MI-IIIs samples (HSG31 and HSG36) and five MI-IIIIs samples (HSG12, HSG15, HSG18, HSG19 and HSG110) plot in the alkaline field

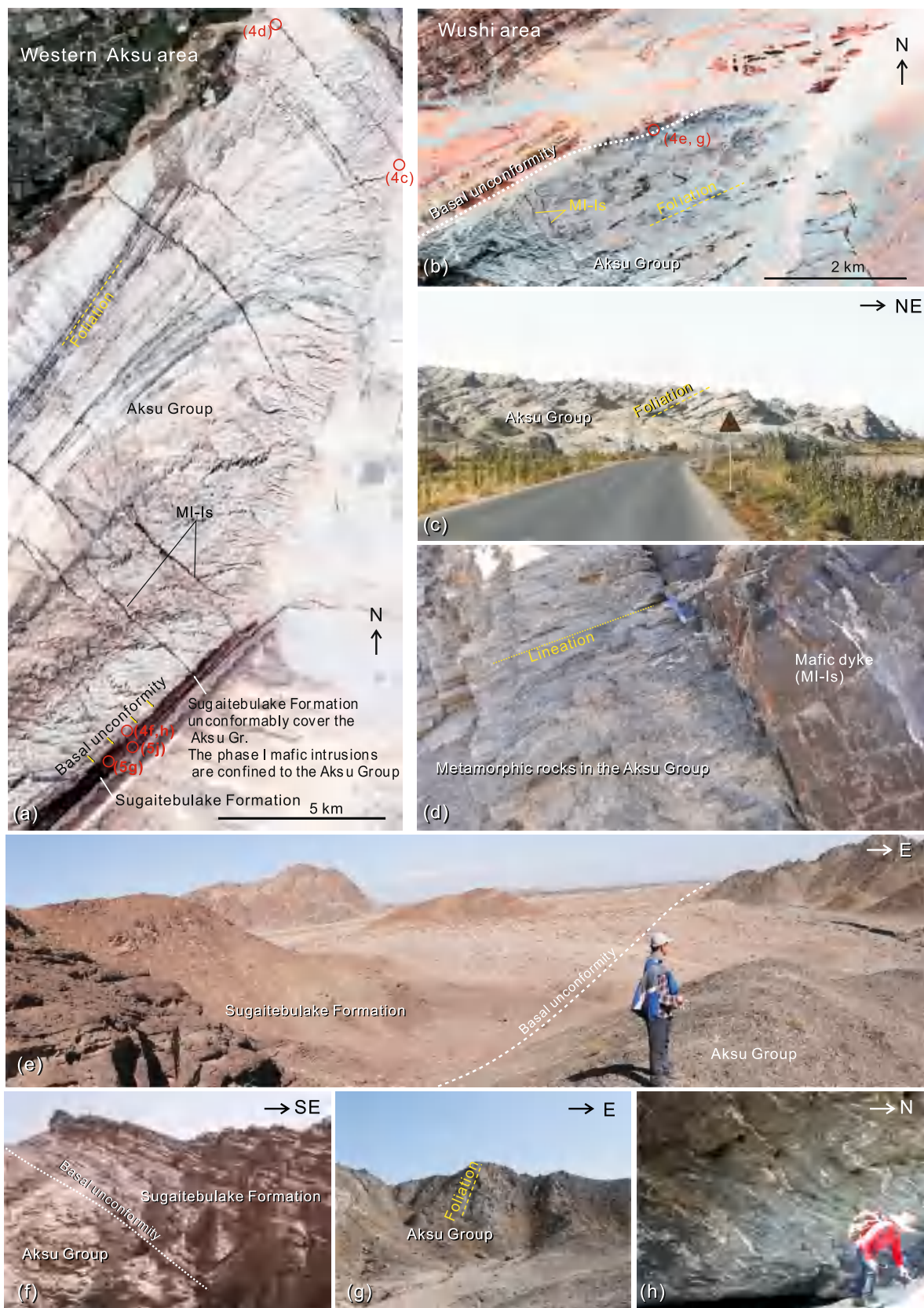


**Fig. 4.** (a) Satellite images of the western Aksu (a) and Wushi (b) regions, showing the deformation features of the Aksu Group and the relationship between the two phases of mafic intrusions; (c) Aksu Group in western Aksu area; (d) Mafic dikes (MI-Is) in the Aksu Group, cutting the deformed schist in Wushi area; (e–f) The contact relationship between the underlying Aksu Group and the overlying Sugaitebulake Formation; (g) Aksu Group in Wushi area; (h) Folds in the Aksu Group schist in southern Aksu area.

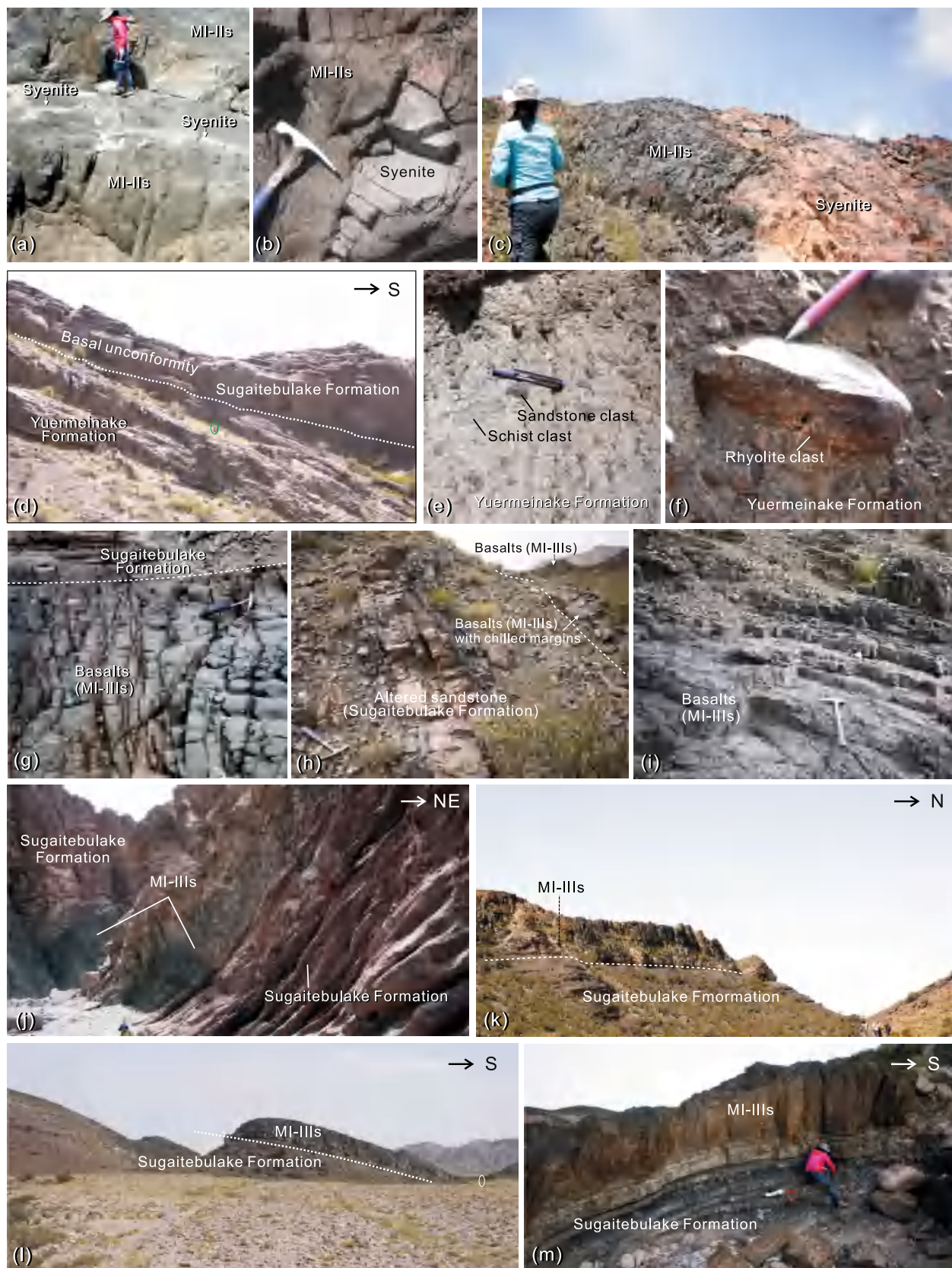


**Fig. 5.** (a–c) Coeval syenite and MI-IIls near the Sugaitebulake village (southern Wushi area); (d) The Sugaitebulake Formation unconformably overlying the Yuermeinake Formation; (e) The conglomerate in the Yuermeinake Formation; (f) Rhyolite clast in the Yuermeinake Formation; (g–j) Basalt layers (MI-IIls) in the Sugaitebulake Formation; (k–m) Mafic sills (MI-IIls) in the Sugaitebulake Formation (southern Aksu area).



**Fig. 6.** Photomicrographs of representative igneous samples. (a–b) Rhyolites; (c) Mafic dikes (MI-Is) in the Aksu Group; (d) Mafic intrusions (MI-IIs) in the Qiaoenbulake Formation; (e, g–h) Basalts (MI-IIIs) in the Sugaitebulake Formation; (f) Mafic sills (MI-IIIs) in the Sugaitebulake Formation; (i–j) Syenites. Sample locations are shown in Fig. 2. Aug-Augite; Or-Orthoclase; Pl-Plagioclase; Px-Pyroxene; Qz- Quartz.

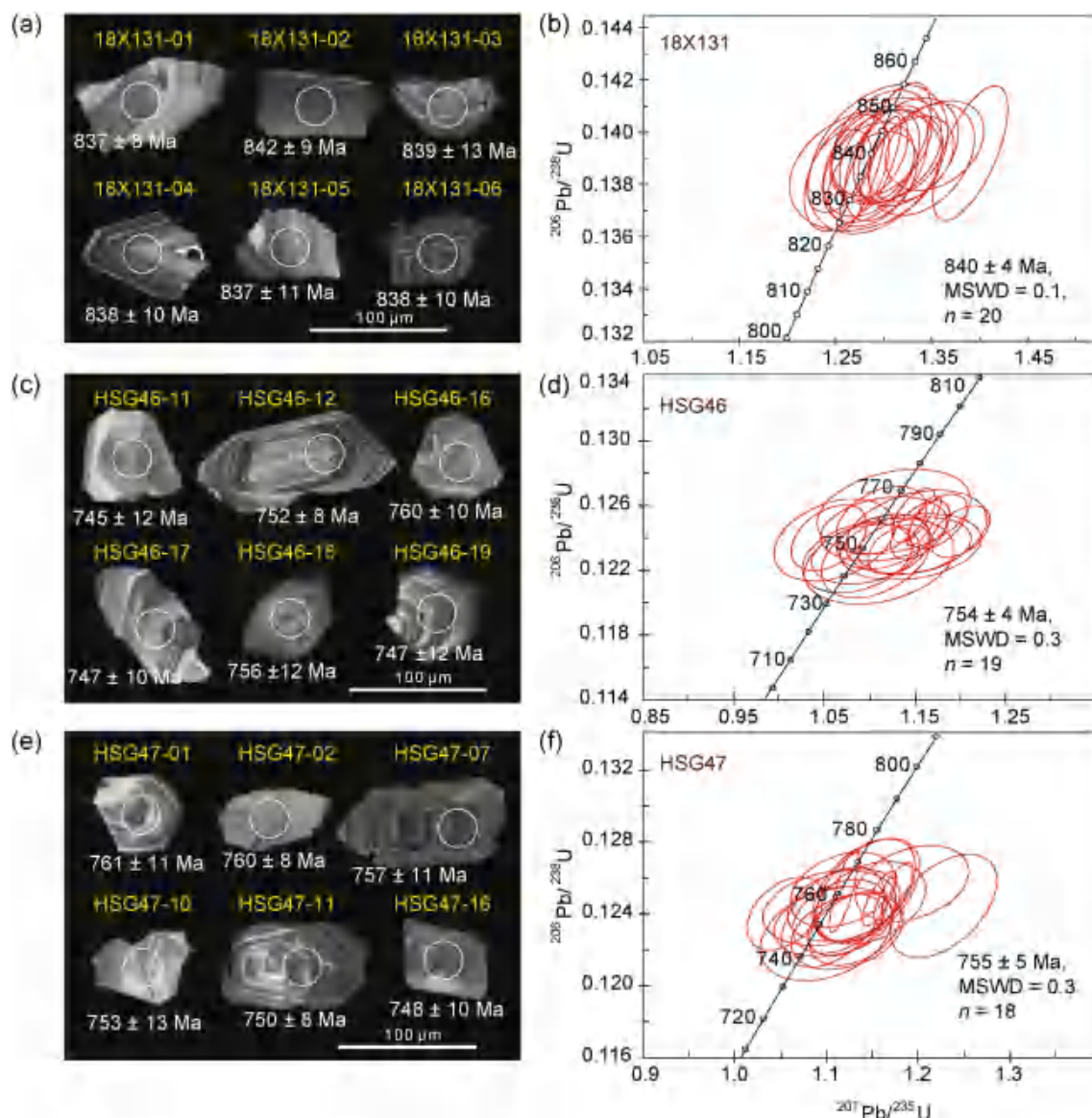


**Fig. 7.** (a, c and e) Cathodoluminescence (CL) images of representative zircon grains showing laser spots in white circle and  $^{206}\text{Pb}/^{238}\text{U}$  ages in white; (b, d and f) Zircon LA-ICPMS U-Pb Concordia ages.

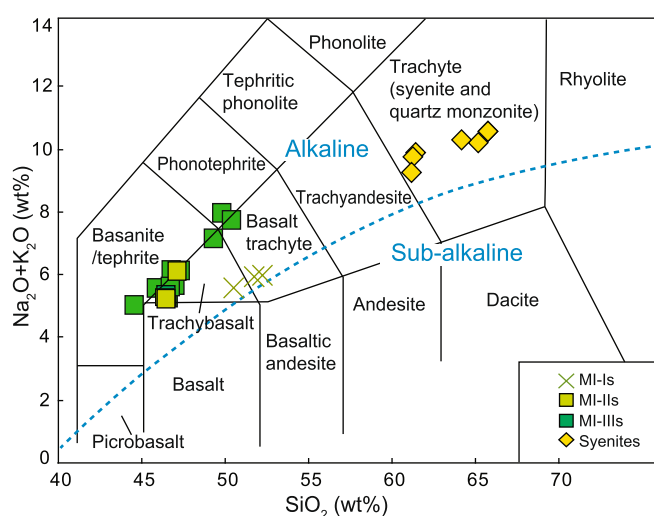


**Fig. 8.** Na<sub>2</sub>O + K<sub>2</sub>O vs. SiO<sub>2</sub> diagram (Middlemost, 1994).

on the (K<sub>2</sub>O + Na<sub>2</sub>O)/SiO<sub>2</sub> diagram (Fig. 8). The MI-IIIs and MI-IIIIs also are enriched in LILEs, but without Nb or Ta anomalies. The distribution patterns of the trace elements resemble ocean island basalts (OIB) (Fig. 10c–f).

The geochemical composition of five syenite samples from Sugaitebulake village are all silica oversaturated (61–66 wt%). They have high (K<sub>2</sub>O + Na<sub>2</sub>O) contents of 9.27–10.55 wt% and plot in the alkaline and trachyte (syenite) fields on the (K<sub>2</sub>O + Na<sub>2</sub>O)/SiO<sub>2</sub> diagram (Fig. 8). On the chondrite-normalized REE diagram, the syenite samples show similar REE patterns with (La/Yb)<sub>N</sub> values ranging from 7 to 16 and Eu/Eu\* values between 0.6 and 1.0 (namely, medium to weak negative Eu anomalies) (Fig. 10c). The negative Eu anomalies likely reflect fractional crystallization of plagioclase feldspar. On the primitive mantle-normalized trace element diagram, the syenites show depletions in Nb, Ta and Ti, and absence of negative Zr and Hf anomalies (Fig. 10d), suggesting residual amphibole and Ti-bearing minerals in the source.

### 5.3. Sr-Nd isotopic composition

Two, 3, 1, 7, and 6 samples of rhyolite clasts, MI-Is, MI-IIIs, MI-IIIIs

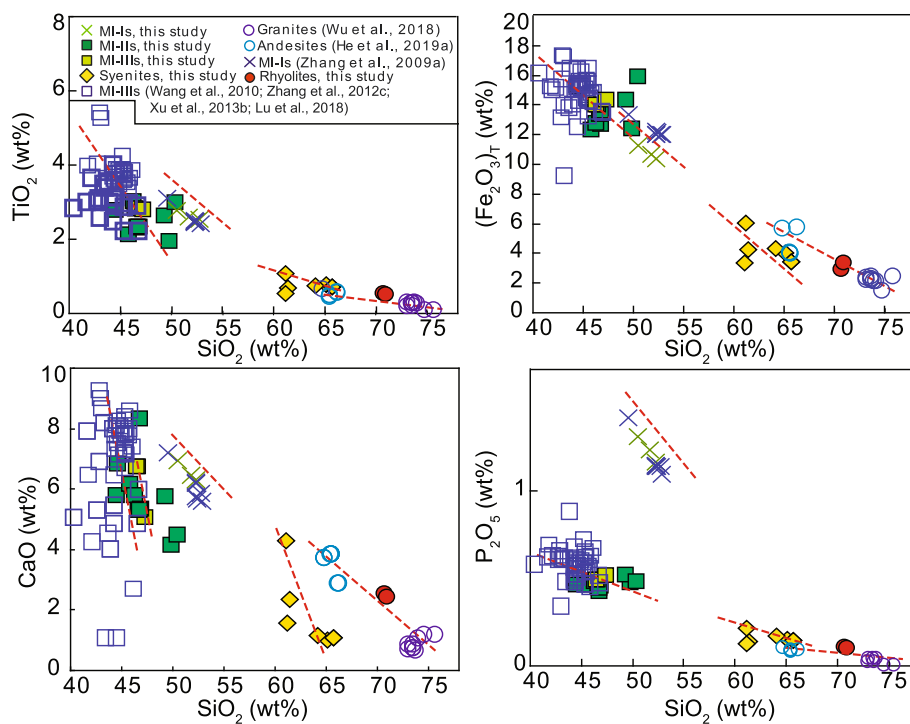


**Fig. 9.** Major oxides  $\text{TiO}_2$ , total  $\text{Fe}_2\text{O}_3$ ,  $\text{CaO}$  and  $\text{P}_2\text{O}_5$  vs.  $\text{SiO}_2$  diagrams. Previous Aksu data sources: granites (Wu et al., 2018), andesites (He et al., 2019a), MI-IIs (Zhang et al., 2009a), MI-IIIs (Wang et al., 2010; Zhang et al., 2012c; Xu et al., 2013b; Lu et al., 2018).

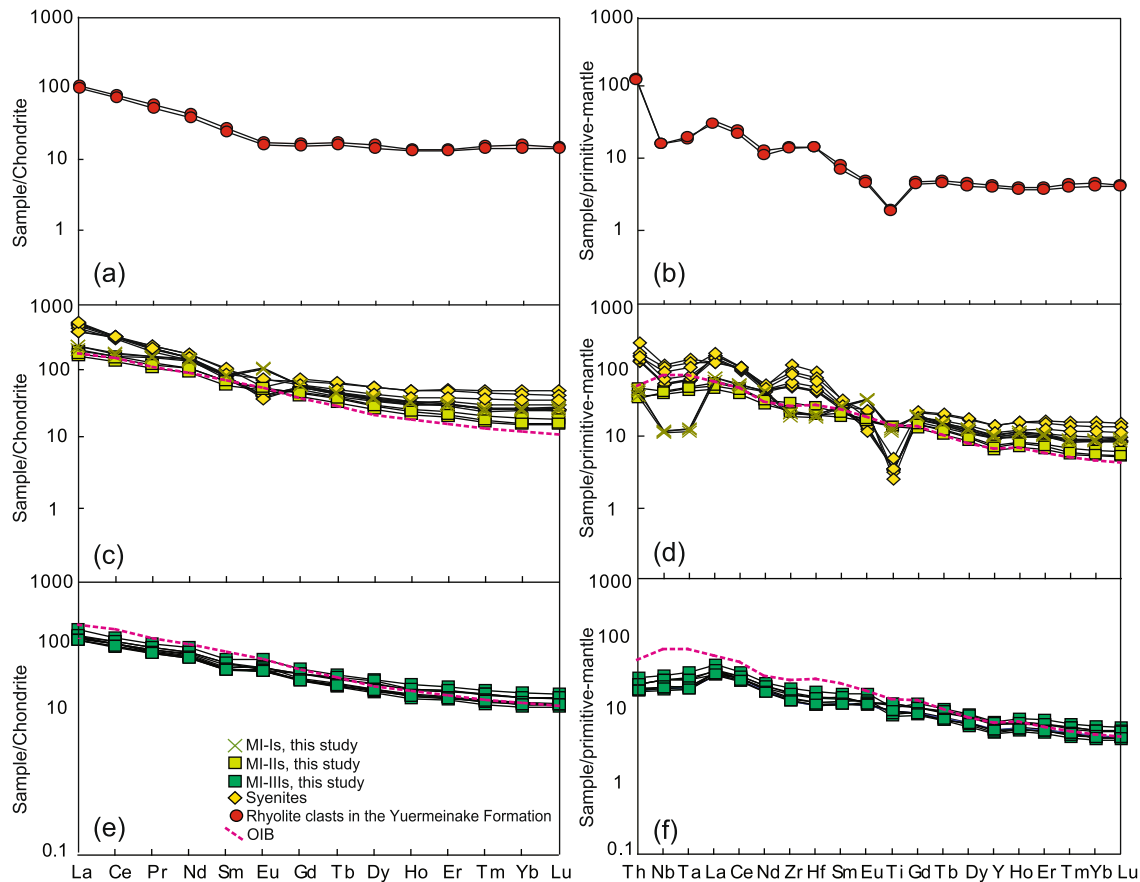


**Fig. 10.** Chondrite-normalized REE patterns (a, c and e) and primitive mantle-normalized multiple trace element diagrams (b, d and f) for samples from the Aksu area. Standard values of chondrite come from Sun and McDonough (1989).

and syenites, respectively, were analyzed for whole-rock Sr-Nd isotopes (Table S3). The rhyolite clasts from the Yuermeinake Formation show uniform Nd isotopic compositions with  $\varepsilon_{\text{Nd}}(t)$  values of  $-1.5$  to  $-1.6$  and initial  $^{87}\text{Sr}/^{86}\text{Sr}$  ratios of  $0.7033$ – $0.7087$ . The syenite samples display a large range of  $^{87}\text{Sr}/^{86}\text{Sr}(t)$  values from  $0.7063$  to  $0.7090$  and near-zero initial  $\varepsilon_{\text{Nd}}(t)$  values from  $-1.8$  to  $0$  (Fig. 11a, Table S3). The emplacement ages of phase I, II and III mafic intrusions are  $\sim 760$ – $745$  Ma (Zhang et al., 2009a; Lu et al., 2018; Xia et al., 2019),  $755$  Ma (coeval with the age of syenite in this study), and  $\sim 520$  Ma (e.g., Lu et al., 2018), respectively. The ages ( $745$  Ma,  $755$  Ma and  $520$  Ma) are used to calculate initial Sr-Nd isotopic ratios. The MI-Is contain a narrow range of radiogenic  $^{87}\text{Sr}/^{86}\text{Sr}(i)$  from  $0.7050$  to  $0.7074$  and unradiogenic  $^{143}\text{Nd}/^{144}\text{Nd}$  with initial  $\varepsilon_{\text{Nd}}(t)$  values ranging from  $0.9$  to  $1.5$  (Fig. 11a, Table S3). The MI-IIs sample shows a  $^{87}\text{Sr}/^{86}\text{Sr}(i)$  of  $0.7076$  and a near-zero initial  $\varepsilon_{\text{Nd}}(t)$  value of  $-0.2$  (Fig. 11a, Table S3). The MI-IIIs contain a large range of  $^{87}\text{Sr}/^{86}\text{Sr}(i)$  values from  $0.7057$  to  $0.7090$  and initial  $\varepsilon_{\text{Nd}}(t)$  values from  $-4.4$  to  $-1.2$  (Fig. 11a, Table S3).

## 6. Discussion

### 6.1. Petrogenesis

Petrological and geochemical data indicate that the  $\sim 840$  Ma rhyolites in the Yuermeinake Formation are sub-alkaline rocks (Fig. 8). They are enriched in LREEs, LILEs, and undepleted in HREE which implies that pyroxene and/or amphibole were present and garnet was absent in the source region. The negative Nb, Ta and Ti anomalies and the absence of negative Zr, Hf, Sm anomalies suggest that these rocks underwent fractionation of amphibole and rutile/titanite but lack significant fractionation of zircon (Fig. 10b). The rhyolites have slightly

negative  $\varepsilon_{\text{Nd}}(t)$  ( $t = 840$  Ma) values of  $-1.5$  to  $-1.6$  and moderate initial  $^{87}\text{Sr}/^{86}\text{Sr}$  ratios (Fig. 11a, Table S3), which are consistent with derivation from lower continental crust rather than oceanic slab.

Intergrowth contacts exist between the syenites and MI-IIIs (Figs. 2, 5a–c), suggesting that these two lithomembers formed coevally ( $754$ – $755$  Ma). The MI-Is yielded a similar crystallization age of  $\sim 760$ – $745$  Ma (Zhang et al., 2009a; Lu et al., 2018; Xia et al., 2019) to the MI-IIIs. In contrast, the MI-IIIs yielded a much younger crystallization age of  $\sim 520$  Ma (Lu et al., 2018). This is consistent with the field occurrences presented earlier in this paper. It further corroborates our argument for at least three phases of mafic igneous activity in the Aksu region with distinct petrogenetic characteristics (Figs. 2, 3 and 4a–b). This conclusion is also supported by whole-rock compositions and Sr-Nd isotopes. In the  $\text{SiO}_2$  vs. major oxides diagrams, the MI-Is belong to different trends or fields from the MI-IIIs and MI-IIIs (Fig. 9). Moreover, in both the rare earth element and trace element diagrams, MI-Is are distinguishable from the MI-IIIs and MI-IIIs (Fig. 10c–f). The MI-Is have positive Eu anomaly and are depleted in Nb and Ta (Fig. 10d). Note that the MI-IIIs and MI-IIIs belong to two different phases of mafic magmatism formed in different times, although they show a similar decreasing trend in Ti,  $\text{Fe}_2\text{O}_3$ , Ca and P with increasing  $\text{SiO}_2$  (Fig. 9), rare earth element and trace element patterns (Fig. 10c–f).

The three phases of mafic rocks exhibit wide ranges of  $^{87}\text{Sr}/^{86}\text{Sr}(i)$  values (between  $0.7050$  and  $0.7074$  for the MI-Is,  $0.7076$  for the MI-IIIs, and  $0.7057$ – $0.7090$  for the MI-IIIs). The variations in the  $^{87}\text{Sr}/^{86}\text{Sr}(i)$  values may reflect: (1) either mantle source heterogeneities or mantle source mixing because the  $^{87}\text{Sr}/^{86}\text{Sr}(i)$  values are not fractionated during partial melting (e.g., Hole et al., 1995); (2) post-emplacement alteration or; (3) contamination by continental crust or input of a subduction zone component (e.g., Wooden et al., 1993). Post-emplacement

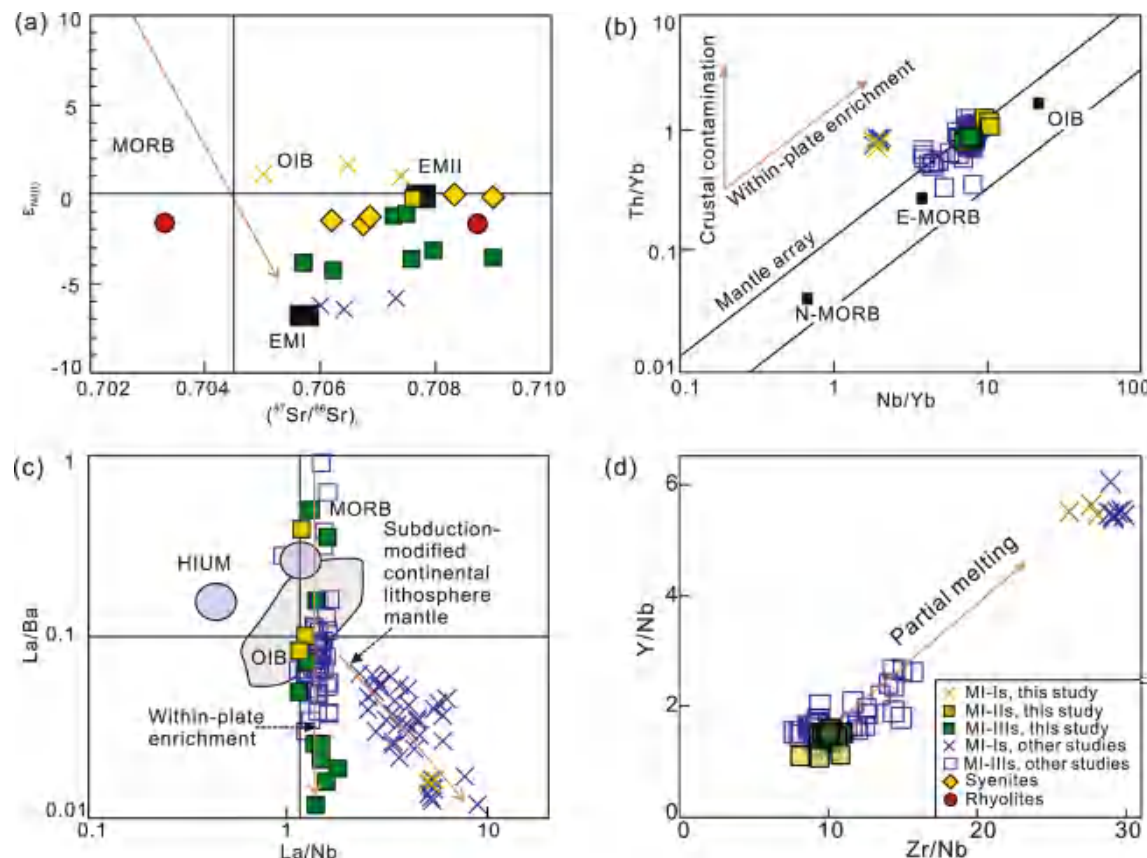


**Fig. 11.** (a)  $\varepsilon_{\text{Nd}}(t)$  vs.  $(^{87}\text{Sr}/^{86}\text{Sr})_i$  diagram, MORB and OIB data are from Woodhead et al. (1998), Nowell et al. (1998) and Pearce et al. (1999); (b)  $(\text{Th/Yb})$  vs.  $(\text{Nb/Yb})$  diagram (Pearce, 1983); (c)  $(\text{La/Ba})$  vs.  $(\text{La/Nb})$  diagram (after Saunders et al., 1992); (d) The diagram of  $\text{Y/Nb}$  vs.  $\text{Zr/Nb}$ . Previous data sources: MI-Is (Zhang et al., 2009a), MI-IIIs (Wang et al., 2010; Zhang et al., 2012c; Xu et al., 2013b; Lu et al., 2018).

alteration should contain chlorite, sericite or albite along with high LOI values. Based on the petrographic analysis and LOI values, the MI-Is samples lack post-emplacement alteration features. The MI-IIs and MI-IIIs have LOI values of 2.76–4.33 and 1.88–4.42, respectively. Thus, the post-emplacement alteration is likely the reason for various  $^{87}\text{Sr}/^{86}\text{Sr}$ (i) values of these samples (Fig. 6c–h and Table S2).

Ratios of Nb/U, Nb/La, Th/Nb, and Th/Ta are relatively unaffected by partial melting or fractional crystallization and are effective discriminants for crustal contamination (e.g., Shellnutt et al., 2014). MI-IIs have Nb/U (26.5–35.6), Nb/La (0.8–0.9), Th/Nb (0.1), and Th/Ta (1.5–2). MI-IIIs have Nb/U (22.3–38.6), Nb/La (0.5–0.9), Th/Nb (0.1), and Th/Ta (1.7–2). These ratios are different from average upper crustal ratios that are 8.9, 0.8, 0.4, and 4.8, respectively (Taylor and McLennan, 1995). The MI-Is have Nb/U (10.9–12.8), Nb/La (0.2), Th/Nb (0.4–0.5), and Th/Ta (6.4–7.1), are comparable to the average upper crust. Hence, we suggest that crustal contamination affected the MI-Is magmas (e.g., Zhang et al., 2012d) and resulted in more radiogenic  $^{87}\text{Sr}/^{86}\text{Sr}$  ratios. In contrast, crustal contamination is a relatively minor contributor to the MI-II and MI-III magmas.

Subduction zone contaminants (oceanic crust, fluids and sediments) are also a potential source of Sr isotopic enrichment. The 0.9 Ga arc-affinity rocks in the Aksu area formed in a subduction setting (He et al., 2019a). The MI-Is display a negative Nb-Ta anomaly (Fig. 10d), which is common in subduction-contaminated magmas. However, these features are absent in MI-IIs and MI-IIIs (Fig. 10c, d). Modification of mafic magma by subduction zone enrichment would produce higher and more variable Ba/La (e.g., Davidson, 1987). MI-Is have high Ba/La values (62–65), indicating a subduction-related arc setting. Contamination by continental crust or subduction zone enrichment would lead to a higher Th value (Pearce, 1983). On diagrams of Th/Yb versus Nb/Yb (Fig. 11b) and La/Ba versus La/Nb (Fig. 11c), the MI-Is fall into the crustal or subduction contamination setting field. Hence, it is likely that the MI-Is formed by crustal or subduction contamination, with magma source derived from the lithospheric mantle or metasomatized mantle wedge. Alternatively, the parental magma of MI-Is was derived from a subduction-related metasomatized subcontinental lithosphere mantle (Zhang et al., 2011, 2012d), which has more radiogenic  $^{87}\text{Sr}/^{86}\text{Sr}$  ratios.

In a comparison between  $\varepsilon_{\text{Nd}}(\text{t})$  versus  $^{87}\text{Sr}/^{86}\text{Sr}$ (i), MI-IIs are close to the compositions of EMII, and MI-IIIs plot close to the compositions of OIB, EMI and EMII (Fig. 11a). Variations in these  $^{87}\text{Sr}/^{86}\text{Sr}$ (i) ratios are likely caused by mantle source heterogeneities or mantle source mixing. On diagrams of Th/Yb-Nb/Yb (Fig. 11b) and La/Ba-La/Nb (Fig. 11c), MI-IIs and MI-IIIs plot along the trend array between OIB and MORB/E-MORB. Thus, the geochemical and isotopic data suggest that the parental magma of the MI-IIs and MI-IIIs formed initially from an enriched OIB asthenospheric mantle source. These magmas were locally modified by interactions with lithospheric mantle containing EMI/EMII-like geochemical characteristics. In a diagram of Y/Nb versus Zr/Nb (Fig. 11d, e.g., Volkert et al., 2015), the MI-IIIs follow a trend with increasing Zr/Nb and a higher degree of melting. The MI-Is and MI-IIs show non-linear trend as compared to the MI-IIIs.

Syenite is an intermediate alkaline rock and common in rift-related tectonic settings (Abdalla et al., 1996). It can be generated by partial melting of crustal rocks (e.g., Lubala et al., 1994; Huang and Wyllie, 1975), extensive fractional crystallization of mantle-derived basaltic magma (Brown and Becker, 1986; Yang et al., 2005), or mixing of alkaline or basic melt with silica melt (e.g., Barker et al., 1975; Shepard, 1995; Zhao et al., 1995; Riishuus et al., 2005). In places, the Aksu syenites are associated with the MI-IIs (Figs. 2, 5a–c). The major elements of the syenites show a distinct decrease of TiO<sub>2</sub>, Fe<sub>2</sub>O<sub>3</sub>, CaO, and P<sub>2</sub>O<sub>5</sub> with increasing SiO<sub>2</sub> (Fig. 9), which is broadly consistent with fractional crystallization. Sr and Nd isotopes are not fractionated during partial melting, so variations in these ratios probably reflect mantle source heterogeneities or mantle source mixing (e.g., Hole et al., 1995). The syenites and associated MI-IIs show similar Sr and Nd isotopic compositions (Fig. 11a). These observations indicate that the syenite

was sourced from the same region as the phase II mafic rocks, and they evolved from the same mantle-derived basaltic magma via fractional crystallization.

## 6.2. Tectonic settings of the igneous rocks

In a diagram of A/NK versus A/CNK (Fig. 12a), the rhyolite samples plot in the metaluminous and I-type granitoid series fields similar to those of arc-affinity rocks (e.g., Pearce et al., 1984; Maniar and Piccoli, 1989). Trace elements serve as proxies that aid in the discrimination between various tectonic settings, particularly a distinction between non-arc and arc environments. Generally, subduction-related arc igneous rocks are characterized by relative depletion in Nb and Ta and enrichment in LREEs and Th. All the rhyolite samples in the present study have remarkable negative Nb-Ta anomalies, Th enrichment and steep LREE and flat HREE patterns (Fig. 10a, b). They have Th/Ta ratios of 11.6–12.7 and plot in the active continental margin field in the Th/Ta vs. Yb diagram (Gorton and Schandl, 2000) (Fig. 12b). The arc-affinity signatures indicate the rhyolite formed in an active continental margin arc setting. The detrital zircon grains in the Yuermeinake Formations are predominantly euhedral with oscillatory zoning, implying their igneous origin and short-distance transportation (He et al., 2014). The U-Pb geochronology data of these detrital zircon grains presented a large age cluster peaking at ~850 Ma (He et al., 2014), comparable with the ages of the rhyolite clasts. Records in the immature sedimentary rocks combined with the geochemical signatures of their igneous counterparts suggest that the ~840 Ma arc magmatism took place near the Aksu region.

Previous studies of ~900 Ma andesites (He et al., 2019a) and ~850 Ma granites (Wu et al., 2018) near Aksu exhibit metaluminous and I-type granitoid characteristics (Fig. 12a). Most of those samples plot in or near the continental margin arc setting (Fig. 12b). Our results, combined with previous data, suggest that Early-Middle Neoproterozoic arc-related magmatic rocks were formed through slab subduction in/near the Aksu region.

Evidence for subduction is well-documented in the blueschist-bearing Aksu Group. The Aksu blueschists represent relict oceanic crust that subducted to mantle-lithospheric depths during the mid-Neoproterozoic (Yong et al., 2013; Xia et al., 2019). Combined with data from the 900–840 Ma intermediate-acid igneous rocks (He et al., 2019a; this study) and the ~760–745 Ma mafic dikes (Zhang et al., 2009a; Lu et al., 2018; Xia et al., 2019), we conclude that Aksu area was the locus of long-lasting subduction during the Early- to Mid-Late-Neoproterozoic (900 Ma to >760–745 Ma).

The coeval MI-Is (~760–745 Ma) and MI-IIs-syenites (755 Ma) intruded into the Aksu Group and Qiaoenbulake Formation, respectively (Fig. 3). The mafic-syenitic suite is usually associated with extensional regimes (Abdalla et al., 1996; Mingram et al., 2000). The emplacement and occurrence of the Late Neoproterozoic Aksu igneous rocks (MI-Is, MI-IIs and syenites) support their association with an extensional continental setting. Several discrimination diagrams were employed to constrain the tectonic setting of these igneous samples. On diagrams of Nb-Zr-Y (Fig. 12c) (Meschede, 1986), the MI-Is plot in the field of volcanic-arc basalt, MI-IIs plot along the “within-plate” alkalic-tholeiitic basalt field (Fig. 12c). The syenite samples (755–754 Ma) plot in the field of the within-plate volcanic zone on the Th/Ta vs. Yb diagram, similar to the MI-IIs (Fig. 12b). Following exhumation of the blueschist-bearing Aksu Group, the region was transformed from an ocean-continent subduction regime to a continental setting during which the MI-Is and MI-IIs were intruded. Under such conditions, magmatic source of the MI-Is series was modified by subduction-related components or alternatively, the MI-Is rocks were derived from the subduction-modified metasomatized subcontinental lithosphere mantle (Zhang et al., 2011). In contrast, the magmatic source of the MI-IIs was unaltered. The mafic rocks (755 Ma) and other coeval magmatism in Tarim are generally thought to reflect continental extension events within the

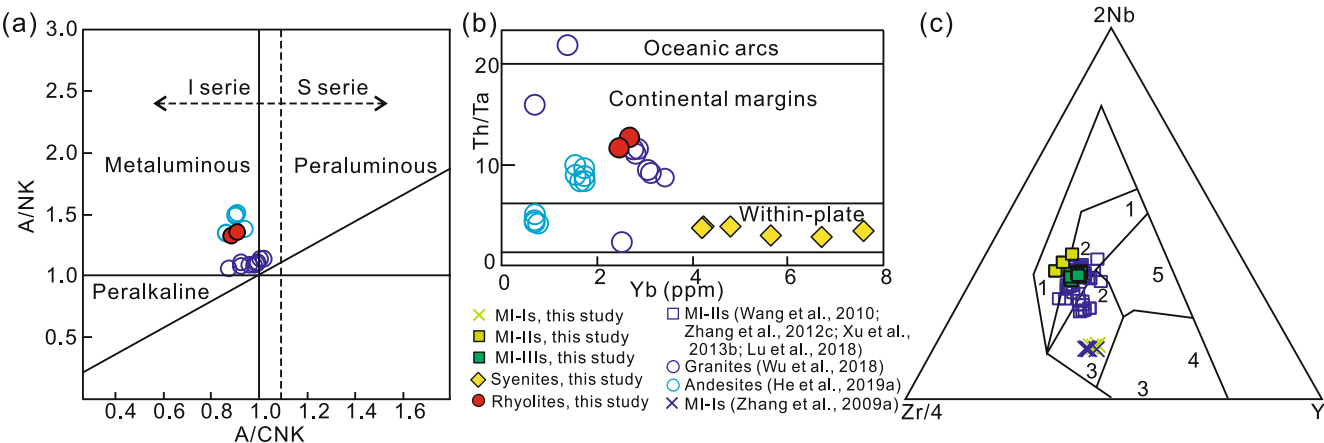


**Fig. 12.** (a) Shand's index of A/NK vs. A/CNK diagram (after Maniar and Piccoli, 1989); (b) Th/Ta vs. Yb discriminant diagram (Gorton and Schandl, 2000); (c) Diagram of Nb-Zr-Y (Meschede, 1986) for Aksu mafic intrusions. 1, within-plate alkalic basalt; 2, within-plate tholeiitic basalt; 3, volcanic-arc basalt; 4, N (normal) MORB; 5, P (plume) MORB. Previous data sources: MI-Is (Zhang et al., 2009a), MI-IIIs (Wang et al., 2010; Zhang et al., 2012c; Xu et al., 2013b; Lu et al., 2018), granite from Wu et al. (2018), and andesite from He et al. (2019a).

Rodinia supercontinent (e.g., Chen et al., 2004; Zhang et al., 2009a, 2009b). Although Late Neoproterozoic normal faulting has no surface expression in the area, seismic profiles indicate the presence of the normal faults in the northwestern Tarim basin. These steeply-dipping normal faults are overlain by Cambrian-aged sedimentary cover (He

et al., 2019b). The basal unit at the western end of the Aksu cliff-face section is thicker relative to the eastern end, which also reveals that normal faults may have been active in the region during the late Neoproterozoic (Turner, 2010).

The MI-IIIs (Wang et al., 2010; Zhang et al., 2012c; this study) in the

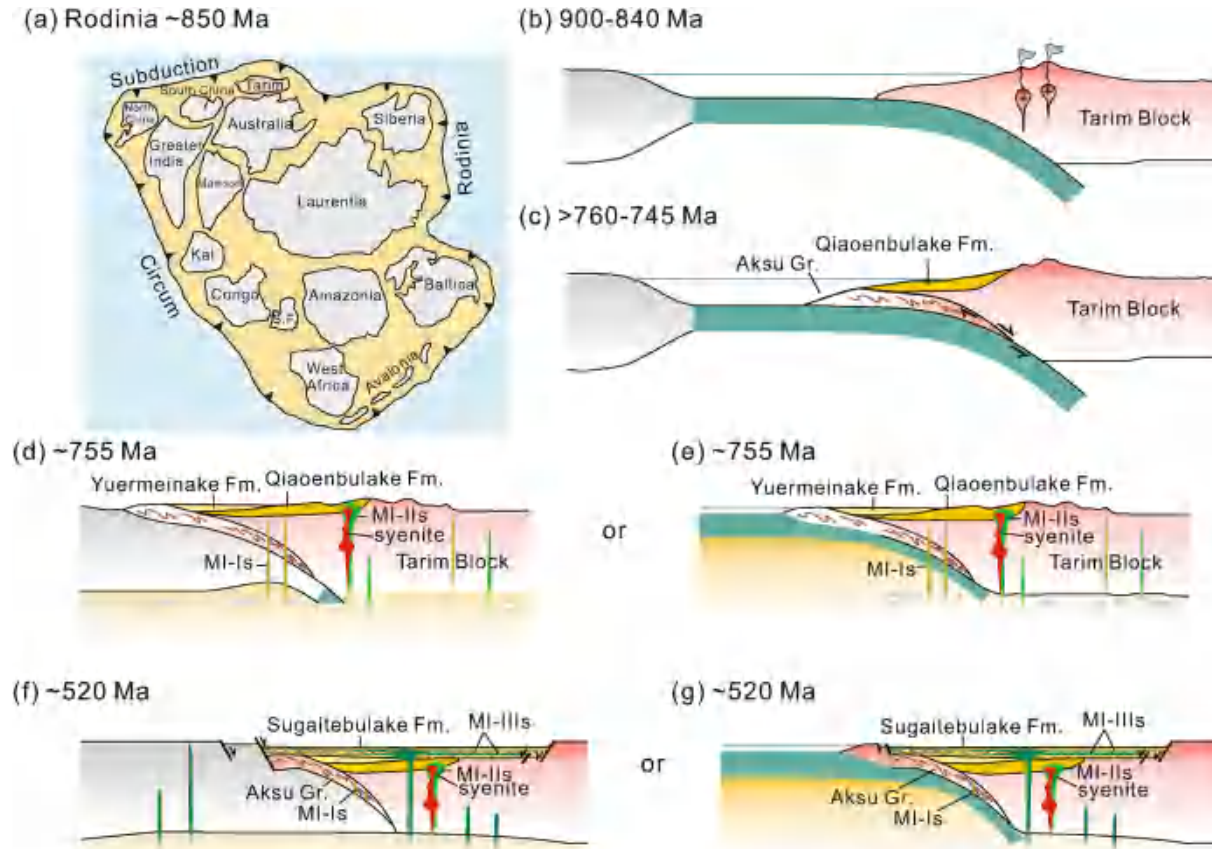


**Fig. 13.** Proposed tectonic evolution of the Tarim Block during the Neoproterozoic. (a) Simplified Rodinia model at ca. 850 Ma with Tarim located at the periphery of the supercontinent (modified after Cawood et al., 2013); (b) Between 900 and 840 Ma, subduction of oceanic lithosphere occurred along the margins of northwestern Tarim (modified after Ge et al., 2016); (c) >760–745 Ma, oceanic crust (including the Aksu Group) subducted beneath the Tarim Block and formed blueschist-facies metamorphic rocks (modified after Ge et al., 2016; Lu et al., 2018); (d–e) At ca. 755 Ma, the Aksu region underwent extension as evidenced by the emplacements of MI-Is and MI-IIIs/syenites into the Aksu Group and Qiaoenbulake Formation, respectively; (d) Modified after Zhang et al. (2013a); (e) Modified after Lu et al. (2018); (f–g) At ~520 Ma, the Tarim crust underwent further extension and basin development. The MI-IIIs were sourced from the upwelling asthenosphere and intruded into the syn-extensional basin.

nonmarine Sugaitebulake Formation exhibit features typical of continental rifts. It is also supported by the geochemical data. On diagrams of Nb-Zr-Y (Fig. 12c) (Pearce and Norry, 1979), the MI-IIIs plot in the area of “within-plate” alkalic-tholeiitic basalt field (Fig. 12c) similar to volcanic rocks associated with continental rift (e. g., Pearce and Norry, 1979).

### 6.3. Tectonic implications

Early Neoproterozoic granitoids are extensive along the margin of the Tarim Craton (Xu et al., 2005, 2013a; Zhang et al., 2006, 2007, 2009a, 2011; Lu et al., 2008; Shu et al., 2011; Long et al., 2011b; Wu et al., 2012, 2018; Wang et al., 2013, 2015). In the Altyn region (southeastern Tarim Block) (Fig. 1), the Early Neoproterozoic granitoids show features of active continental margin magmatic rocks (Wang et al., 2013). In the Kuluketage region (northeastern Tarim Block) (Fig. 1), the Mid- to Late-Neoproterozoic high-grade facies metamorphic rocks indicate an advancing-type accretion processes (He et al., 2013; Ge et al., 2016). Tectonothermal events, combined with the Early Neoproterozoic magmatic rocks and blueschists in the Aksu region (Liou et al., 1989, 1996; Nakajima et al., 1990; Zhu et al., 2011; Yong et al., 2013; Wu et al., 2018; He et al., 2019a; Xia et al., 2019; this study), suggest that the northern and southeastern parts of Tarim Block were active continental margins during the Early to Middle Neoproterozoic, which might be associated with the peripheral subduction-accretion process during the assembly of the Rodinia supercontinent (Fig. 13a–c) (e.g., Lu et al., 2018; Long et al., 2011b; Zhang et al., 2012a; Ge et al., 2016).

Numerous Mid- to Late Neoproterozoic mafic dikes and rift-related igneous rocks are identified in the Kuluketage and Korla regions (northeastern Tarim Block) (e.g., Xu et al., 2005; Shu et al., 2011; Zhang et al., 2007, 2009b, 2012a, 2013a; Long et al., 2011a, 2012; Long et al., 2011b), Tiekklik (southwestern Tarim Block) (e.g., Wang et al., 2015), Aksu (northwestern Tarim Block) (Zhu et al., 2008; Zhang et al., 2009a; Wang et al., 2010; this paper), and drill cores in the central Tarim basin (e.g., Xu et al., 2013a). These rocks were regarded as by-products of rifting events in the Tarim Block (Zhang et al., 2012a; Xu et al., 2013a, 2013b). Some mafic and ultramafic rocks show arc-like geochemical signatures (e.g., Zhang et al., 2012d), thus, a mantle plume-plate subduction interaction (Zhang et al., 2012a, 2012d) or an accretionary orogen (Ge et al., 2014c, 2016) model were employed to explain their formation.

The Early to Mid-Neoproterozoic subduction described above likely led to the closure of an ocean along the present-day Aksu region. From a geochemical perspective, we are unable to discern what blocks may have collided with Tarim (if any) during this interval (Fig. 13d). Furthermore, if evidence for this collision is available, it is buried beneath thick Phanerozoic cover.

Alternatively, some argue that magmatism was related to long-lived subduction along the margins of Tarim (e. g., Ge et al., 2016). In this scenario, the Tarim block was located along the periphery of the Rodinia supercontinent and its margins were part of the circum-Rodinia subduction zone (Fig. 13e). If this is the case, the rift-related MI-Is, MI-IIs and syenites might be triggered by a Neoproterozoic plume beneath the Rodinia supercontinent (Fig. 13e).

Regarding the MI-IIIs, Wang et al. (2010) and Zhang et al. (2012c) show typical continental rifting features both in field occurrence and geochemistry. We argue that the MI-IIIs were sourced from the upwelling asthenosphere and intruded into the syn-extensional basin. The formation of the MI-IIIs series rocks corresponds to the Late Neoproterozoic - Early Cambrian rifting event developed on the northern margin of the Tarim Block which isolated the Tarim Block from neighboring crustal fragments (e.g., Turner, 2010).

Our new data, along with previously published results, lead us to propose a tentative tectonic model for the Tarim Block: (1) Between 900 and 840 Ma, subduction occurred along the margins of northwestern

Tarim (Fig. 13b). (2) At >760–745 Ma (constrained by the ages of syenites in this study, and mafic dikes in Zhang et al., 2009a, Lu et al., 2018, Xia et al., 2019), oceanic crust (including the Aksu Group) subducted beneath the Tarim Block and formed blueschist-facies metamorphic rocks (Fig. 13c). (3) At 755 Ma, the Tarim Block underwent extension as evidenced by the emplacement of MI-Is and MI-IIs (Fig. 13d or e). (4) At ~520 Ma (Lu et al., 2018), the Tarim crust underwent further extension and basin development (Fig. 13f or g).

## 7. Concluding remarks

This study focused on the field observations, geochronology and geochemistry of three phases of Middle Neoproterozoic - Early Cambrian mafic intrusions, syenites, and rhyolite clasts in the Aksu area, northwestern Tarim Block. Geochemical and Sr-Nd isotopic data suggest that the ~840 Ma rhyolite clasts in the Yuermeinake Formation conglomerates were formed in a subduction-related arc setting. In contrast, the MI-Is (~760–745 Ma) and MI-IIs (755 Ma) were derived from an enriched lithospheric mantle, with MI-Is metasomatized by subduction-related components. We suggest that the transition from subduction-related convergence to continental rifting occurred around 760 Ma in the northwestern Tarim Block. The MI-IIIs magmatism (~520 Ma) represents further later extension event occurred in the Tarim Block.

## CRediT authorship contribution statement

**Zhihui Cai:** Formal analysis, Investigation, Data curation, Visualization, Writing - original draft. **Bizhu He:** Formal analysis, Investigation, Writing - original draft. **Joseph G. Meert:** Writing - review & editing. **Xuxuan Ma:** Formal analysis, Data curation, Visualization, Writing - original draft. **Cunli Jiao:** Formal analysis, Investigation, Writing - original draft. **Ruohan Liu:** Investigation, Formal analysis. **Xijie Chen:** Data curation. **Xiaorui Yun:** Investigation.

## Declaration of Competing Interest

The authors declare that they have no known competing financial interests or personal relationships that could have appeared to influence the work reported in this paper.

## Acknowledgments

We are much indebted to two anonymous reviewers for their perceptive and constructive comments. Thanks due to Editor Guochun Zhao for his efficient handling and encouragement on this manuscript. This work was co-supported by the National Key Research and Development Project ‘Key scientific issues of transformative technology’ (2019YFA0708601), the Key Special Project for Introduced Talents Team of the Southern Marine Science and Engineering Guangdong Laboratory (Guangzhou) (GML2019ZD0201), the second Tibetan Plateau Scientific Expedition and Research Program (STEP) Grant (2019QZKK0802, 2019QZKK0901), the National Science Foundation of China (No. 41872121, 41502198, 41572180, 41302166, 41403029 and 41472198), the Fund from the Key Laboratory of Deep-Earth Dynamics of Ministry of Natural Resources (No. J1901-20-4), Scientific Research Fund of the Institute of Geology, Chinese Academy of Geological Sciences (S2003, J2024), the Basic Research Project of Chinese Academy of Geological Sciences (No. JYYWF20180903, JYYWF20182103), the open fund of State Key Laboratory for Mineral Deposits Research at Nanjing University (2020-LAMD-K04), and the Geological Survey project of China (No. DD20190006, DD20190057, DD20190059, DD20190060). All cited data are available in referenced publications.

## Appendix A. Supplementary data

Supplementary data to this article can be found online at <https://doi.org/10.1016/j.precamres.2021.106278>.

[org/10.1016/j.precamres.2021.106278](https://doi.org/10.1016/j.precamres.2021.106278).

## References

- Abdalla, J.A., Said, A.A., Visonà, D., 1996. New geochemical and petrographic data on the Gabbro-Syenite Suite between Hargeysa and Berbera-Shiikh (northern Somalia). *J. Asian Earth Sci.* 23 (3), 363–373.
- Barker, F., Wones, D.R., Sharp, W.N., Desborough, G.A., 1975. The Pikes Peak batholith, Colorado Front Range, and a model for the origin of the gabbro-anorthosite-syenite-potassic granite suite. *Precambr. Res.* 2, 97–160.
- Brown, P.E., Becker, S.M., 1986. Fractionation, hybridisation and magma-mixing in the Kialineqcentre East Greenland. *Contrib. Miner. Petrol.* 92, 57–70.
- Cai, Z.H., Jiao, C.L., He, B.Z., Qi, L.X., Ma, X.X., Cao, Z.C., Xu, Z.Q., Chen, X.J., Liu, R.H., 2020. Archean-Paleoproterozoic tectonothermal events in the central Tarim Block: constraints from granitic gneisses revealed by deep drilling wells. *Precambr. Res.* 347, 105776.
- Cai, Z.H., Ma, X.X., He, B.Z., 2019. The initial assembly of the Chinese Central Tianshan, Yili and Tarim blocks to the Rodinia supercontinent prior to the Early Neoproterozoic? *Acta Geol. Sin.* 93, 2426–2445 (in Chinese with English abstract).
- Cai, Z.H., Xu, Z.Q., Yu, S.Y., Li, S.Z., He, B.Z., Ma, X.X., Chen, X.J., Xu, X.Y., 2018. Neoarchean magmatism and implications for crustal growth and evolution of the Kuluketage region, northeastern Tarim Craton. *Precambr. Res.* 304, 156–170.
- Cawood, P.A., Wang, Y.J., Xu, Y.J., Zhao, G.C., 2013. Locating South China in Rodinia and Gondwana: a fragment of greater India lithosphere? *Geology* 8, 903–906.
- Chen, Y., Xu, B., Zhan, S., Li, Y., 2004. First mid-Neoproterozoic paleomagnetic results from the Tarim Basin (NW China) and their geodynamic implications. *Precambr. Res.* 133, 271–281.
- Davidson, J.P., 1987. Crustal contamination versus subduction zone enrichment: examples from the Lesser Antilles and implications for mantle source compositions of island arc volcanic rocks. *Geochim. Cosmochim. Acta* 51 (8), 2185–2198.
- Gao, J., Wang, X.S., Klemd, R., Jiang, T., Qian, Q., Mu, L.X., Ma, Y.Z., 2015. Record of assembly and breakup of Rodinia in the Southwestern Altaiids: evidence from Neoproterozoic magmatism in the Chinese Western Tianshan Orogen. *J. Asian Earth Sci.* 113, 173–193.
- Gao, L.Z., Guo, X.P., Ding, X.Z., Zong, W.M., Gao, Z.J., Zhang, C.H., Wang, Z.Q., 2013. Nanhuan glaciation event and its stratigraphic correlation in Tarim Plate, China. *Acta Geol. Sin.* 34, 39–57.
- Gao, Z.J., Chen, K.Q., 2003. The Nanhua system of Xinjiang and some geological issues of Nanhua system in China. *Geological Survey Research* 26, 8–13 (in Chinese with English abstract).
- Ge, R.F., Zhu, W.B., Wilde, S.A., Kemp, A.I.S., Jeon, H., Martin, L.A.J., Zhu, W.B., Wu, H. L., 2020. Generation of Eoarchean continental crust from altered mafic rocks derived from a chondritic mantle: The ~3.72 Ga Aktash gneisses, Tarim Craton (NW China). *Earth Planet. Sci. Lett.* 538 (2020), 116225.
- Ge, R.F., Zhu, W.B., Wilde, S.A., Wu, H.L., 2018. Remnants of Eoarchean continental crust derived from a subducted proto-arc. *Sci. Adv.* 4 eaao3159.
- Ge, R.F., Zhu, W.B., Wilde, S.A., 2016. Mid-Neoproterozoic (ca. 830–800 Ma) metamorphic P-T paths link Tarim to the circum-Rodinia subduction-accretion system. *Tectonics* 35 (6), 1465–1488.
- Ge, R.F., Zhu, W.B., Wilde, S.A., He, J.W., Cui, X., 2015. Synchronous crustal growth and reworking recorded in late Paleoproterozoic granitoids in the northern Tarim craton: in situ zircon U-Pb-Hf-O isotopic and geochemical constraints and tectonic implications. *Geol. Soc. Am. Bull.* 127, 781–803.
- Ge, R.F., Zhu, W.B., Wilde, S.A., Wu, H.L., He, J.W., Zheng, B.H., 2014a. Archean magmatism and crustal evolution in the northern Tarim Craton: insights from zircon U-Pb-Hf-O isotopes and geochemistry of ~2.7 Ga orthogneiss and amphibolite in the Korla Complex. *Precambr. Res.* 252, 145–165.
- Ge, R.F., Zhu, W.B., Wilde, S.A., He, J.W., 2014b. Zircon U-Pb-Lu-Hf-O isotopic evidence for ≥3.5 Ga crustal growth, reworking and differentiation in the northern Tarim Craton. *Precambr. Res.* 249, 115–128.
- Ge, R.F., Zhu, W.B., Wilde, S.A., He, J.W., Cui, X., Wang, X., Zheng, B.H., 2014c. Neoproterozoic to Paleozoic long-lived accretionary orogeny in the northern Tarim Craton. *Tectonics* 33, 302–329.
- Gorton, M.P., Schandl, E.S., 2000. From continents to island arcs: a geochemical index of tectonic setting for arc-related and within-plate felsic to intermediate volcanic rocks. *Can. Mineral.* 38, 1065–1073.
- He, B.Z., Jiao, C.L., Cai, Z.H., Liu, R.H., Meert, J.G., Yun, X.R., Wang, T.Y., Chen, W.W., Yu, Z.Y., Li, J.C., Peng, S.T., Hao, G.M., Guo, X.P., Qiao, X.F., 2021. Soft-sediment deformation structures (SSDS) in the Ediacaran and lower Cambrian succession of the Aksu area, NW Tarim Basin, and their implications. *Palaeogeogr. Palaeocl.* 567 (2021), 110237.
- He, J.Y., Xu, B., Li, D., 2019a. Newly discovered early Neoproterozoic (ca. 900 Ma) andesitic rocks in the northwestern Tarim Craton: Implications for the reconstruction of the Rodinia supercontinent. *Precambr. Res.* 325, 55–68.
- He, B.Z., Jiao, C.L., Huang, T.Z., Zhou, X.G., Cai, Z.H., Cao, Z.C., Jiang, Z.Z., Cui, J.W., Yu, Z.Y., Chen, W.W., Liu, R.H., Yun, X.R., Hao, G.M., 2019b. Structural architecture of Neoproterozoic rifting depression groups in the Tarim Basin and their formation dynamics. *Sci. China, Ser. D Earth Sci.* 62 (3), 45–65.
- He, J.W., Zhu, W.B., Ge, R.F., Zheng, B.H., Wu, H.L., 2014. Detrital zircon U-Pb ages and Hf isotopes of Neoproterozoic strata in the Aksu area, northwestern Tarim Craton: implications for supercontinent reconstruction and crustal evolution. *Precambr. Res.* 254, 194–209.
- He, Z.Y., Zhang, Z.M., Zong, K.Q., Dong, X., 2013. Paleoproterozoic crustal evolution of the Tarim Craton: constrained by zircon U-Pb and Hf isotopes of meta-igneous rocks from Korla and Dunhuang. *J. Asian Earth Sci.* 78 (12), 54–70.
- Hole, M.J., Saunders, A.D., Rogers, G., Sykes, M.A., 1995. The relationship between alkaline magmatism, lithospheric extension and slab window formation along continental destructive plate margins. In: Smellie, J.L. (Ed.), *Volcanism Associated with Extension at Consuming Plate Margins*. Geol. Soc. Spec. Publ., pp. 265–285.
- Hoskin, P.W.O., Schaltegger, U., 2003. The composition of zircon and igneous and metamorphic petrogenesis. *Rev. Mineral. Geochem.* 53, 27–62.
- Hou, K.J., Li, Y.H., Tian, Y.Y., 2009. In situ U-Pb zircon dating using laser ablation multi ion counting-ICP-MS. *Min. Depos.* 28 (4), 481–492 (in Chinese with English abstract).
- Hou, K.J., Li, Y.H., Zou, T.R., Qu, X.M., Shi, Y.R., Xie, G.Q., 2007. Laser ablation-MC-ICP-MS technique for Hf isotope microanalysis of zircon and its geological applications. *Acta Petrol. Sin.* 23 (10), 2595–2604.
- Hu, A.Q., Wei, G.J., 2006. On the age of the Neo-Archean Qingir Gray Gneisses from the Northern Tarim Basin, Xinjiang, China. *Acta Geol. Sin.* 80, 126–134 (in Chinese with English Abstract).
- Huang, W.L., Wyllie, P.J., 1975. Melting reaction in the system NaAlSi<sub>3</sub>O<sub>8</sub>-KAlSi<sub>3</sub>O<sub>8</sub>-SiO<sub>2</sub> to 35 kilobars, dry and with excess water. *J. Geol.* 83, 737–748.
- Jackson, S.E., Pearson, N.J., Griffin, W.L., Belousova, E.A., 2004. The application of laser ablation-inductively coupled plasma-mass spectrometry to in situ U-Pb zircon geochronology. *Chem. Geol.* 211, 47–69.
- Jia, C., 1997. In: *Structural Geology and Petroleum Potential in the Tarim Basin, China*. Petroleum Industry Press House, Beijing, p. 438.
- Lei, R.X., Wu, C.Z., Chi, G.X., Gu, L.X., Dong, L.H., Qu, X., Jiang, Y.H., Jiang, S.Y., 2013. The Neoproterozoic Hongliujing A-type granite in Central Tianshan (NW China): LA-ICP-MS zircon U-Pb geochronology, geochemistry, Nd-Hf isotope and tectonic significance. *Precambr. Res.* 74, 142–154.
- Lei, R.X., Wu, C.Z., Gu, L.X., Zhang, Z.Z., Chi, G.X., Jiang, Y.H., 2011. Zircon U-Pb chronology and Hf isotope of the Xingxingxia granodiorite from the Central Tianshan zone (NW China): implications for the tectonic evolution of the southern Altaiids. *Gondwana Res.* 20, 582–593.
- Liou, J.G., Tsujimori, T., Zhang, R.Y., Katayama, I., Maruyama, S., 2004. Global UHP metamorphism and continental subduction/collision: the Himalayan model. *Int. Geol. Rev.* 46, 1–27.
- Liou, J.G., Graham, S.A., Maruyama, S., Zhang, R.Y., 1996. Characteristics and tectonic significance of the late Proterozoic Aksu blueschists and diabasic dikes northwest Xinjiang China. *Int. Geol. Rev.* 38, 228–244.
- Liou, J.G., Graham, S.A., Mayuyama, S., Wang, X., Xiao, X., Carroll, A.R., Chu, J., Feng, Y., Hendrix, M.S., Liang, Y.H., McKnight, C.L., Tang, Y., Wang, Z.X., Zhao, M., Zhu, B., 1989. Proterozoic blueschist belt in western China: best documented Precambrian blueschists in the world. *Geology* 17, 1127–1131.
- Liu, Y.S., Gao, S., Hu, Z.C., Gao, C.G., Zong, K.Q., Wang, D.B., 2010. Continental and oceanic crust recycling-induced melt-peridotite interactions in the Trans-North China Orogen: U-Pb dating, Hf isotopes and trace elements in zircons from mantle xenoliths. *J. Petrol.* 51, 537–571.
- Long, X.P., Sun, M., Yuan, C., Kröner, A., Hu, A.Q., 2012. Zircon REE patterns and geochemical characteristics of Paleoproterozoic anatexic granite in the northern Tarim Craton, NW China: implications for the reconstruction of the Columbia supercontinent. *Precambr. Res.* 222–223, 474–487.
- Long, X.P., Yuan, C., Sun, M., Xiao, W.J., Zhao, G.C., Zhou, K.F., Wang, Y.J., Hu, A.Q., 2011a. The discovery of the oldest rocks in the Kuluketage area and its geological implications. *Sci. China Ser. D: Earth Sci.* 54, 342–348.
- Long, X.P., Yuan, C., Sun, M., Kröner, A., Zhao, G.C., Wilde, S., Hu, A.Q., 2011b. Reworking of the Tarim Craton by underplating of mantle plume-derived magmas: Evidence from Neoproterozoic granitoids in the Kuluketage area, NW China. *Precambr. Res.* 187, 1–14.
- Long, X.P., Yuan, C., Sun, M., Zhao, G.C., Xiao, W.J., Wang, Y.J., Yang, Y.H., Hu, A.Q., 2010. Archean crustal evolution of the northern Tarim Craton, NW China: Zircon U-Pb and Hf isotopic constraints. *Precambr. Res.* 180, 272–284.
- Lu, S.N., Li, H.K., Zhang, C.L., Niu, G.H., 2008. Geological and geochronological evidence for the Precambrian evolution of the Tarim Craton and surrounding continental fragments. *Precambr. Res.* 160, 94–107.
- Lu, Y.Z., Zhu, W.B., Jourdan, F., Ge, R.F., Cui, X., Wen, B., 2018. <sup>40</sup>Ar/<sup>39</sup>Ar ages and geological significance of Neoproterozoic Cambrian mafic rocks in the Aksu Wushi area, NW Tarim Craton. *Geol. J.* 54, 1–18.
- Lubala, R.T., Frick, C., Roders, J.H., Walraven, F., 1994. Petrogenesis of syenites and granites of the Schiel Alkaline complex, Northern Transvaal, South Africa. *J. Geol.* 102, 307–309.
- Ludwig, K.R., 2003. Isoplot/Ex Version 3.0: a Geochronological Toolkit for Microsoft Excel. Berkeley Geochronology Center, Berkeley, CA.
- Lv, P., Yu, S.Y., Peng, Y.B., Zhang, J., Xie, W.M., Jiang, X.Z., Gao, X.Y., Ji, W.T., Li, S.Z., Liu, Y.J., 2020. Paleoproterozoic multiple magmatic-metamorphic events in the Dunhuang Block, eastern Tarim Craton: Implications for assembly of the Columbia supercontinent. *Precambr. Res.* 351, 105949.
- Ma, X.X., Shu, L.S., Meert, J.G., Xu, Z.Q., 2014. The fingerprint of Precambrian basement in the Chinese Central Tianshan: evidence from inherited/xenocrystic zircons of magmatic rocks. *Geol. Mag.* 1–8.
- Ma, X.X., Shu, L.S., Santos, M., Li, J.Y., 2013. Paleoproterozoic collisional orogeny in Central Tianshan: assembling the Tarim Block within the Columbia supercontinent. *Precambr. Res.* 228, 1–19.
- Ma, X.X., Shu, L.S., Santos, M., Li, J.Y., 2012. Detrital zircon U-Pb geochronology and Hf isotope data from Central Tianshan suggesting a link with the Tarim Block: implications for Proterozoic supercontinent history. *Precambr. Res.* 206–207, 1–16.
- Maniar, P.D., Piccoli, P.M., 1989. Tectonic discrimination of granitoids. *Geol. Soc. Am. Bull.* 101, 635–643.

- Meert, J.G., 2014. Strange attractors, spiritual interlopers and lonely wanderers: The search for pre-Pangean supercontinents. *Geosci. Front.* 5 (2), 155–166.
- Meschede, M., 1986. A method of discriminating between different types of midocean ridge basalts and continental tholeiites with the Nb–Zr–Y diagram. *Chem. Geol.* 56, 207–218.
- Middlemost, E.A.K., 1994. Naming materials in the magma/igneous rock system. *Earth Sci. Rev.* 37, 215–224.
- Mingram, B., Trumbull, R.B., Littman, S., Gerstenberger, H., 2000. A petrogenetic study of anorogenic felsic magmatism in the Cretaceous Paresis ring complex, Namibia: evidence for mixing of crust and mantle-derived components. *Lithos* 54 (1–2), 1–22.
- Nakajima, T., Maruyama, S., Uchiumi, S., Liou, J.G., Wang, X., Xiao, X., Graham, S.A., 1990. Evidence for late Proterozoic subduction from 700-Myr-old blueschists in China. *Nature* 346, 263–265.
- Nowell, G.M., Kempton, P.D., Noble, S.R., Fitton, J.G., Saunders, A.D., Mahoney, J.J., Taylor, R.N., 1998. High precision Hf isotope measurements of MORB and OIB by thermal ionization mass spectrometry: insights into the depleted mantle. *Chem. Geol.* 149, 211–233.
- Pearce, J.A., Kempton, P.D., Nowell, G.M., Noble, S.R., 1999. Hf–Nd element and isotope perspective on the nature of provenance of mantle and subduction components in the western Pacific arc-basin systems. *J. Petrol.* 40, 1579–1611.
- Pearce, J.A., Harris, N.W., Tindle, A.G., 1984. Trace element discrimination diagrams for the tectonic interpretation of granitic rocks. *J. Petrol.* 25, 956–983.
- Pearce, J.A., 1983. Role of the sub-continental lithosphere in magma genesis at active continental margins. In: Hawkesworth, C.J., Norry, M.J. (Eds.), *Continental Basalts and Mantle Xenoliths*. Shiva, Nantwich, pp. 230–249.
- Pearce, J.A., Norry, M.J., 1979. Petrogenetic implications of Ti Zr, Y, and Nb variations in volcanic rocks. *Contrib. Miner. Petrol.* 69, 33–47.
- Peng, Y.B., Yu, S.Y., Li, S.Z., Zhang, J.X., Liu, Y.S., Li, Y.S., Santosh, M., 2019. Early Neoproterozoic magmatic imprints in the Altun–Qilian–Kunlun region of the Qinghai–Tibet Plateau: Response to the assembly and breakup of Rodinia supercontinent. *Earth Sci. Rev.* 199, 102954.
- Ren, R., Guan, S.W., Zhang, S.C., Wu, L., Zhang, H.Y., 2020. How did the peripheral subduction drive the Rodinia breakup: constraints from the Neoproterozoic tectonic process in the northern Tarim craton. *Precambr. Res.* 339 (2020), 105612.
- Riishuus, M.S., Peate, D.W., Tegner, C., Wilson, J.R., Brooks, C.K., Waught, T.E., 2005. Petrogenesis of syenites at a rifted continental margin: origin, contamination and interaction of alkaline mafic and felsic magmas in the Astrophyllite Bay Complex, East Greenland. *Contrib. Miner. Petrol.* 149, 350–371.
- Saunders, A.D., Storey, M., Kent, R.W., Norry, M.J., 1992. Consequences of plume–lithosphere interactions. In: Storey, B.C., Alabaster, T., Pankhurst, R.J. (Eds.), *Magmaatism and the Cause of Continental Breakup*. Geol. Soc. London, Spec. Publ., pp. 41–60.
- Shellnutt, J.G., Bhat, G.M., Wang, K.L., Brookfield, M.E., Jahn, B.M., Dostal, J., 2014. Petrogenesis of flood basalts from the Early Permian Panjal Traps, Kashmir, India: geochemical evidence for shallow melting of the mantle. *Lithos* 204, 159–171.
- Sheppard, S., 1995. Hybridization of shoshonitic lamprophyre and calc-alkaline granite magma in the Early Proterozoic Mt. Bunney igneous suite, Northern Territory. *Aust. J. Earth Sci.* 42, 173–185.
- Shu, L.S., Deng, X.L., Zhu, W.B., Ma, D.S., Xiao, W.J., 2011. Precambrian tectonic evolution of the Tarim Block, NW China: new geochronological insights from the Quruqtagh domain. *J. Asian Earth Sci.* 42, 774–790.
- Sun, S.S., McDonough, W.F., 1989. Chemical and isotopic systematics of oceanic basalts: implications for mantle composition and processes. In: Saunders, A.D., Norry, M.J. (Eds.), *Magmaatism in the Ocean Basins*. Geol. Soc. London, Spec. Publ., pp. 313–345.
- Taylor, S.R., McLennan, S.M., 1995. The geochemical evolution of the continental crust. *Rev. Geophys.* 33, 241–265.
- Turner, S.A., 2010. Sedimentary record of Late Neoproterozoic rifting in the NW Tarim Basin, China. *Precambr. Res.* 181, 85–96.
- Volkert, R.A., Feigenson, M.D., Mana, S., Bolge, L., 2015. Geochemical and Sr–Nd isotopic constraints on the mantle source of Neoproterozoic mafic dikes of the rifted eastern Laurentian margin, north-central Appalachians, USA. *Lithos* 212–215, 202–213.
- Wang, C., Liu, L., Wang, Y.H., He, S.P., Li, R.S., Li, M., Yang, W.Q., Cao, Y.T., Collins, A. S., Shi, C., Wu, Z.N., 2015. Recognition and tectonic implications of an extensive Neoproterozoic volcano-sedimentary rift basin along the southwestern margin of the Tarim Craton, northwestern China. *Precambr. Res.* 257, 65–82.
- Wang, C., Wang, Y.H., Liu, L., He, S.P., Li, R.S., Li, M., Yang, W.Q., Cao, Y.T., Meert, J.G., Shi, C., 2014a. The Paleoproterozoic magmatic–metamorphic events and cover sediments of the Tielikeli Belt and their tectonic implications for the southern margin of the Tarim Craton, northwestern China. *Precambr. Res.* 254, 210–225.
- Wang, P., Zhao, G., Liu, R., Han, Y., Yao, J., Li, J., 2020. Zircons from the Tarim basement provide insights into its position in Columbia and Rodinia supercontinents. *Precambr. Res.* 341 (2020), 105621.
- Wang, X.S., Gao, J., Klemd, R., Jiang, T., Li, J.L., Zhang, X., Tan, Z., Li, L., Zhu, Z.X., 2014b. Geochemistry and geochronology of the Precambrian high-grade metamorphic complex in the Southern Central Tianshan ophiolitic mélange, NW China. *Precambr. Res.* 254, 129–148.
- Wang, B., Shu, L.S., Liu, H.S., Gong, H.J., Ma, Y.Z., Mu, L.X., Zhong, L.L., 2014c. First evidence for ca. 780 Ma intra-plate magmatism and its implications for Neoproterozoic rifting of the North Yili Block and tectonic origin of the continental blocks in SW of Central Asia. *Precambr. Res.* 254, 258–272.
- Wang, C., Liu, L., Yang, W., Zhu, X., Cao, Y., Kang, L., Chen, S., Li, R., He, S., 2013. Provenance and ages of the Altyn Complex in Altyn Tagh: Implications for the early Neoproterozoic evolution of northwestern China. *Precambr. Res.* 230, 193–208.
- Wang, F., Wang, B., Shu, L.S., 2010. Continental tholeiitic basalt of the Akesu area (NW China) and its implication for the Neoproterozoic rifting in the northern Tarim. *Acta Geol. Sin.* 26 (2), 547–558 (in Chinese with English abstract).
- Wen, B., Evans, D.A.D., Li, Y.-X., 2017. Neoproterozoic paleogeography of the Tarim block: An extended or alternative “missing link” model for Rodinia? *Earth Planet Sci. Lett.* 458, 92–106.
- Wen, B., Evans, D.A.D., Li, Y., Wang, Z., Liu, C., 2015. Newly discovered Neoproterozoic diamictite and cap carbonate (DCC) couplet in Tarim Craton, NW China: Stratigraphy, geochemistry, and paleoenvironment. *Precambr. Res.* 271, 278–294.
- Wooden, J.L., Czamanske, G.K., Fedorenko, V.A., Arndt, N.T., Chauvel, C., Bouse, R.M., King, B.S.W., Knight, R.J., Seims, D.F., 1993. Isotopic and trace-element constraints on mantle and crustal contributions to Siberian continental flood basalts, Noril'sk area, Siberia. *Geochim. Cosmochim. Acta* 57, 3677–3704.
- Woodhead, J.D., Eggins, S.M., Johnson, R.W., 1998. Magma genesis in the New Britain island arc: further insights into melting and mass transfer processes. *J. Petrol.* 39, 1641–1668.
- Wu, G.H., Chen, Z.Y., Qu, T.L., Xu, Y.L., Zhang, C.Z., 2012. SHRIMP zircon age of the high aeromagnetic anomaly zone in central Tarim Basin and its geological implications. *Nat. Sci.* 4, 1–4.
- Wu, G.H., Xiao, Y., Bonin, B., Ma, D.B., Li, X., Zhu, G.Y., 2018. Ca. 850 Ma magmatic events in the Tarim Craton: age, geochemistry and implications for assembly of Rodinia supercontinent. *Precambr. Res.* 305, 489–503.
- XBGMR, 1966. 1: 200000 Geological map of RPC, Wushi sheet (K-44-XXVI). Chinese National 543 Publishing House, Xinjiang.
- Xia, B., Zhang, L.F., Du, Z.X., Xu, B., 2019. Petrology and age of Precambrian Aksu blueschist, NW China. *Precambr. Res.* 326, 295–311.
- Xu, B., Jian, P., Zheng, H.F., Zou, H.B., Zhang, L.F., Liu, D.Y., 2005. U–Pb zircon geochronology and geochemistry of Neoproterozoic volcanic rocks in the Tarim Block of northwest China: implications for the breakup of Rodinia supercontinent and Neoproterozoic glaciations. *Precambr. Res.* 136, 107–123.
- Xu, Z.Q., He, B.Z., Zhang, C.L., Zhang, J.X., Wang, Z.M., Cai, Z.H., 2013a. Tectonic framework and crustal evolution of the Precambrian basement of the Tarim Block in NW China: new geochronological evidence from deep drilling samples. *Precambr. Res.* 235, 150–162.
- Xu, B., Zou, H.B., Chen, Y., He, J.Y., Wang, Y., 2013b. The Sugetbrak basalts from northwestern Tarim block of northwest China: Geochronology, geochemistry and implications for Rodinia breakup and ice age in the Late Neoproterozoic. *Precambr. Res.* 236, 214–226.
- Yang, J.H., Chung, S.L., Wilde, S.A., Wu, F.Y., Chu, M.F., Lo, C.H., Fan, H.R., 2005. Petrogenesis of post-orogenic syenites in the Sulu Orogenic Belt, East China: geochronological, geochemical and Nd–Sr isotopic evidence. *Chem. Geol.* 214, 99–125.
- Yang, Y.H., Zhang, H.F., Chu, Z.Y., Xie, L.W., Wu, F.Y., 2010. Combined chemical separation of Lu, Hf, Rb, Sr, Sm and Nd from a single rock digest and precise and accurate isotope determinations of Lu–Hf, Rb–Sr and Sm–Nd isotope systems using Multi-Collector ICP-MS and TIMS. *Int. J. Mass Spectrom.* 290, 120–126.
- Yang, Y.K., Shi, K.B., Liu, B., Qin, S., Wang, J.Q., Zhang, X.F., 2014. Tectono-sedimentary evolution of the Sinian in the Northwest Tarim Basin. *Sci. Geol. Sin.* 49, 19–29 (in Chinese with English abstract).
- Yong, W.J., Zhang, L., Hall, C.M., Mukasa, S.B., Essene, E.J., 2013. The  $^{40}\text{Ar}/^{39}\text{Ar}$  and Rb–Sr chronology of the Precambrian Aksu blueschists in western China. *J. Asian Earth Sci.* 63, 197–205.
- Yu, S.Y., Li, S.Z., Zhang, J.X., Liu, Y.J., Peng, Y.B., Li, Y.S., 2019. Grenvillian orogeny in the Oulongbuluke Block, NW China: Constraints from an ~1.1 Ga Andean-type arc magmatism and metamorphism. *Gondwana Res.* 320, 424–437.
- Yu, S.Y., Zhang, J.X., Real, P.G., Zhao, X.L., Hou, K.J., Gong, J.H., Li, Y.S., 2013. The Grenvillian orogeny in the Altun–Qilian–North Qaidam mountain belts of northern Tibet Plateau: constraints from geochemical and zircon U–Pb age and Hf isotopic study of magmatic rocks. *J. Asian Earth Sci.* 73, 372–395.
- Zeng, L.S., Gao, L.E., Dong, C.Y., Tang, S.H., 2012. High-pressure melting of metapelitic and the formation of Ca-rich granitic melts in the Namche Barwa Massif, southern Tibet. *Gondwana Res.* 21, 138–151.
- Zhang, C.L., Zou, H.B., Li, H.K., Wang, H.Y., 2013a. Tectonic framework and evolution of the Tarim Block in NW China. *Gondwana Res.* 23 (4), 1306–1315.
- Zhang, J.X., Yu, S.Y., Gong, J.H., Li, H.K., Hou, K.J., 2013b. The latest Nearchean–Paleoproterozoic evolution of the Dunhuang block, eastern Tarim craton, northwestern China: Evidence from zircon U–Pb dating and Hf isotopic analyses. *Precambr. Res.* 226, 21–42.
- Zhang, C.L., Li, H.K., Santosh, M., Li, Z.X., Zou, H.B., Wang, H.Y., Ye, H.M., 2012a. Precambrian evolution and cratonization of the Tarim Block, NW China: petrology, geochemistry, Nd-isotopes and U–Pb zircon geochronology from Archaean gabbro–TTG–potassic granite suite and Paleoproterozoic metamorphic belt. *J. Asian Earth Sci.* 47, 5–20.
- Zhang, J.X., Gong, J.H., Yu, S.Y., 2012b. 1.85 Ga HP granulite-facies metamorphism in the Dunhuang block of the Tarim Craton, NW China: evidence from U–Pb zircon dating of mafic granulites. *J. Geol. Soc.* 169, 511–514.
- Zhang, Z.C., Kang, J.L., Kusky, T., Santosh, M., Huang, H., Zhang, D.Y., Zhu, J., 2012c. Geochronology, geochemistry and petrogenesis of Neoproterozoic basalts from Sugetbrak, northwest Tarim block, China: implications for the onset of Rodinia supercontinent breakup. *Precambr. Res.* 220–221, 158–176.
- Zhang, C.L., Zou, H.B., Wang, H.Y., Li, H.K., Ye, H.M., 2012d. Multiple phases of the Neoproterozoic igneous activity in Quruqtagh of the northeastern Tarim Block, NW China: Interaction between plate subduction and mantle plume? *Precambr. Res.* 222–223, 488–502.
- Zhang, C.L., Yang, D.S., Wang, H.Y., Takahashi, Y., Ye, H.M., 2011. Neoproterozoic mafic-ultramafic layered intrusion in Quruqtagh of northeastern Tarim Block, NW

- China: two phases of mafic igneous activity with different mantle sources. *Gondwana Res.* 19, 177–190.
- Zhang, C.L., Li, Z.X., Li, X.H., Ye, H.M., 2009a. Neoproterozoic mafic dyke swarms at the northern margin of the Tarim Block, NW China: age, geochemistry, petrogenesis and tectonic implications. *J. Asian Earth Sci.* 35, 167–179.
- Zhang, Z.Y., Zhu, W.B., Shu, L.S., Su, J.B., Zheng, B.H., 2009b. Neoproterozoic ages of the Kuluketage diabase dyke swarm in Tarim, NW China, and its relationship to the breakup of Rodinia. *Geol. Mag.* 146, 150–154.
- Zhang, C.L., Li, Z.X., Li, X.H., Ye, H.M., 2007. An early Paleoproterozoic high-K intrusive complex in southwestern Tarim Block, NW China: age, geochemistry and implications for the Paleoproterozoic tectonic evolution of Tarim. *Gondwana Res.* 12, 101–112.
- Zhang, C.L., Li, Z.X., Li, X.H., Ye, H.M., Wang, A.G., Guo, K.Y., 2006. Neoproterozoic bimodal intrusive complex in the Southwestern Tarim Block, Northwest China: age, geochemistry, and implications for the rifting of Rodinia. *Int. Geol. Rev.* 48, 112–128.
- Zhao, G.C., Cawood, P.A., 2012. Precambrian geology of China: preface. *Precambr. Res.* 222–223, 13–54.
- Zhao, J.X., Shiraishi, K., Ellis, D.J., Sheraton, J.W., 1995. Geochemical and isotopic studies of syenites from the Yamoto Mountains, East Antarctica: implication for the origin of syenitic magmas. *Geochim. Cosmochim. Acta* 59, 1363–1385.
- Zheng, B.H., Zhu, W.B., Jahn, B.M., Shu, L.S., Zhang, Z.Y., Su, J.B., 2010. Subducted Precambrian oceanic crust: geochemical and Sr-Nd isotopic evidence from metabasalts of the Aksu blueschist, NW China. *J. Geol. Soc. London* 167 (6), 1161–1170.
- Zhu, W.B., Zheng, B.H., Shu, L.S., Ma, D.S., Wu, H.L., Li, Y.X., Huang, W.T., Yu, J.J., 2011. Neoproterozoic tectonic evolution of the Precambrian Aksu blueschist terrane, northwestern Tarim, China: insights from LA-ICP-MS zircon U-Pb ages and geochemical data. *Precambr. Res.* 185 (3–4), 215–230.
- Zhu, W.B., Zhang, Z.Y., Shu, L.S., Lu, H.F., Su, J.B., Yang, W., 2008. SHRIMP U-Pb zircon geochronology of Neoproterozoic Korla mafic dykes in the northern Tarim Block, NW China: implications for the long-lasting breakup process of Rodinia. *J. Geol. Soc. London* 165, 887–890.